Construction and Building Materials 344 (2022) 128167

Contents lists available at ScienceDirect

Construction and Building Materials

journal homepage: www.elsevier.com/locate/conbuildmat

Influence of short glass fibres and spatial features on the mechanical behaviour of weft-knitted textile reinforced concrete elements in bending

Minu Lee *, Jaime Mata-Falcón, Walter Kaufmann

Institute of Structural Engineering, Swiss Federal Institute of Technology (ETH) Zurich, Switzerland

ARTICLE INFO

Keywords:
Textile reinforced concrete
Short integral glass fibres
Shear connectors
Experimental study
Bending
Crack behaviour
KnitCrete

ABSTRACT

Weft-knitted textiles made from high-strength fibrous materials offer great potential for use as a flexible stay-in-place formwork and reinforcement system since they allow creating complex geometries (i.e. doubly curved or folded) and introducing spatial features such as ribs within the fabric. However, the closed surface of the textile and its placement at the bottom edge of the concrete element present major challenges regarding bond, which may lead to premature failure due to delamination of the reinforcement initiated by a substantial opening of a governing crack. This study investigates the influence of short integral glass fibres and spatial bond ribs on the mechanical behaviour of weft-knitted textile reinforced concrete elements subjected to bending and their potential to increase the shear resistance. To this end, an experimental campaign consisting of 14 four-point-bending tests was conducted, where the specimens were examined regarding their load-deformation behaviour, crack kinematics and failure modes. The contribution of the short glass fibres to the load-bearing mechanism was estimated with Pfyl's fibre engagement model, based on the material characterisation results from prism tests on fibre reinforced concrete members. The Tension Chord Model was used to predict the stress-strain relationship of the reinforcement and the crack widths in the constant moment zone, which yielded a good correlation between the predictions and the experiments. The short fibres mostly contributed to the flexural response in the serviceability limit state, but only slightly increased the shear resistance due to their low fibre effectiveness. The introduction of bond shear connectors was shown to be essential to prevent the premature delamination of the reinforcement. The use of tall connectors allowed doubling the bearing capacity with respect to the flat reinforcement without any spatial features, effectively bridging the governing crack and reaching the tensile capacity of the longitudinal textile reinforcement.

1. Introduction

The urgent need for the construction industry to reduce its ecological footprint has led to numerous advances to decrease the volume of concrete consumption. Thereby, the use of conventional steel reinforcing bars presents an intrinsic limitation for lightweight concrete structures due to the minimum concrete cover needed to protect the reinforcement from corrosion (between 20 and 50 mm depending on the regional building codes and exposure). Textile reinforcement allows minimising the thickness of the concrete elements to a few millimetres when using non-corrosive materials such as aramid, carbon or glass fibres [1]. The mechanical behaviour of such fibres is usually linear elastic with high strength (3000–4000 MPa) at a moderate to high stiffness (glass fibre: ca. 70 GPa; carbon fibre: ca. 240 GPa). Textile reinforcement typically consists of rovings formed from multiple filaments, which exhibit lower strength and stiffness than the individual fibres due to several reasons: (i) the failure mode is brittle and does not allow for redistribution of stresses within the roving cross-section once the weakest fibre reaches its tensile strength [2–4]; (ii) commonly used fibres are sensitive to lateral loading and may be damaged due to deviations at the crack edges [5,6]; (iii) the loads are transferred via inter-fibre friction within the rovings, which leads to an inhomogeneous stress distribution over the cross-section [7]; (iv) while the ribs in conventional deformed steel bars provide a proper force transfer between reinforcement and concrete [8], the bond of textile reinforcement mainly relies on adhesion and friction [9–11]. Coating or even fully impregnating the rovings (e.g. with epoxy resin) can attenuate these effects and may significantly improve the mechanical performance of the textile reinforcement [12–14].

Most of the existing studies in the literature and applications in the construction sector make use of woven bi-directional grids of straight rovings, which, however, only allow flat or single curved geometries. In

* Corresponding author.
E-mail addresses: mlee@ethz.ch, lee@ibk.baug.ethz.ch (M. Lee).

https://doi.org/10.1016/j.conbuildmat.2022.128167
Received 16 March 2022; Received in revised form 14 June 2022; Accepted 15 June 2022
Available online 21 June 2022

Nomenclature

Acronyms

Acronym	*Description*
ACDM	Automated Crack Detection and Measurement
AF	Aramid fibre
CF	Carbon fibre
CMO	Crack mouth opening
DIC	Digital Image Correlation
GF	Glass fibre
TCM	Tension Chord Model
TRC	Textile reinforced concrete

Capital latin symbols

Symbol	*Unit Description*
A_t	[mm^2] Cross-sectional area of the textile reinforcement
E_c	[GPa] Young's modulus of the concrete
E_{rov}	[GPa] Young's modulus of a single textile roving
E_t	[GPa] Young's modulus of the textile reinforcement
$E_{t,meas}$	[GPa] Young's modulus of the textile reinforcement measurend in the experiment
M	[kNm] Bending moment
V_f	[%] Volumetric fibre content

Small latin symbols

Symbol	*Unit Description*
a_t	[mm^2/m], Cross-sectional area of the textile reinforcemen per unit width
b	[mm], Width of the specimen
d	[mm], Depth of the reinforcement
f_{ct}	[MPa], Tensile strength of the concrete
$f_{ct,fl}$	[MPa], Flexural tensile strength of the concrete
f_{rov}	[MPa], Tensile strength of a single textile roving
h	[mm], Height of the specimen
l_f	[mm], Fibre length
s_r	[mm], Crack spacing
s_{r0}	[mm], Theoretical maximum crack spacing
$s_{r,meas}$	[mm], Crack spacing measured in the experiment
$s_{r,TCM}$	[mm], Crack spacing predicted with the Tension Chord Model
u_r	[mm], Crack opening
w_r	[mm], Crack mouth opening
$w_{r,meas}$	[mm], Crack mouth opening measured in the experiment
$w_{r,TCM}$	[mm], Crack mouth opening predicted with the Tension Chord Model
x_c	[mm], Depth of the compression zone in the concrete

Greek symbols

Symbol	*Unit Description*
α_{fl}	[-], Ratio of uniaxial tensile strength to flexural tensile strength of the concrete
$\Delta\varepsilon$	[‰], Strain difference due to tension stiffening effect
ε_{cm}	[‰], Mean strains in the concrete
ε_{tm}	[‰], Mean strains in the textile reinforcement
λ	[-], Ratio of actual crack spacing to theoretical maximum crack spacing
ρ_{fl}	[%], Equivalent geometrical reinforcement ratio for members in bending
ρ_t	[%], Geometrical reinforcement ratio
σ_{cf}	[MPa], Effective residual tensile stress offered by the fibres (referred to as effective fibre stress)
σ_{cf0}	[MPa], Effective fibre stress at zero crack width (neglecting fibre activation)
$\sigma_{cf,cr}$	[MPa], Effective fibre stress at cracking
σ_t	[MPa], Tensile stresses in the textile reinforcement
σ_{tu}	[MPa], Stresses in textile reinforcement at ultimate load
τ_b	[MPa], Bond shear stresses at the interface between textile and concrete

contrast, weft-knitted textiles offer the possibility to create complex shapes (i.e. doubly curved or folded) without the need for tedious discretisation and stitching multiple patches together [15]. The KnitCrete technology developed at ETH Zurich [16] exploits the possibilities of weft-knitted textiles in a flexible stay-in-place formwork system. The fabric is tensioned in a scaffolding frame, using cables or bending-active rods as additional supports. The flexible formwork is stiffened by applying a thin layer of either cement paste or epoxy resin to reduce deformations and provide stability during the subsequent casting of the concrete. The feasibility of this construction procedure on an architectural scale was demonstrated in the KnitCandela pavilion in Mexico City [17], which originated from a collaboration of the Block Research Group and Zaha Hadid Architects. However, the integration of reinforcement in spatial structures presents a significant challenge due to the more complex reinforcement layouts and detailing. The use of high-strength fibrous materials for weft-knitted textiles serving as a stay-in-place formwork and reinforcement system may significantly improve the efficiency of concrete structures with complex geometry due to the simplified construction procedure and reduced material consumption, as outlined by the authors in [18]. The potential of this new type of reinforcement and the mechanical behaviour of various knitting patterns, fibre materials and coating types were investigated in tension [19] and bending [20]. These studies concluded that integrating high-strength straight rovings ('inlays') within a knitted base textile made from a non-structural yarn yielded the most beneficial behaviour in terms of strength and stiffness of the textiles. While the introduction of spatial ribs in the knitted textile to enhance the bond between the reinforcement and the concrete significantly improved the post-cracking behaviour in tension by preventing spalling of the concrete cover, most of the textile reinforced concrete elements tested in bending failed due to the formation of a shear crack and a subsequent horizontal delamination crack along the reinforcement, with the ribs breaking out of the concrete.

The addition of short fibres to concrete members with conventional woven textile reinforcement improves the post-cracking behaviour in terms of increased strength and reduced crack widths [21–25], which may also have a beneficial influence on the shear resistance of concrete elements with weft-knitted textile reinforcement. Although the pull-out of the fibres usually results in a softening response with increasing crack opening [26], the residual stresses in the crack may still be sufficient to prevent a premature collapse. Furthermore, various studies in the literature have examined the influence of 3D spacer fabrics on the strength and stiffness of textile reinforced concrete (e.g. [27–29]). The delamination of the reinforcement from the concrete observed in bending tests on concrete members with weft-knitted textile reinforcement [20] may be prevented through the introduction of more pronounced and strengthened spatial ribs acting as shear connectors.

This study presents an experimental campaign investigating the influence of integral short glass fibres and spatial features in the textile, i.e. various rib geometries, on the mechanical behaviour of weft-knitted textile reinforced concrete elements in bending. A total of 14 specimens were tested in four-point bending, which allows assessing the response in the tension chord from digital image correlation measurements in the constant moment zone (as described by the authors in [20]) and a detailed analysis of the crack pattern and kinematics. The effect of the short fibres on the load-bearing behaviour of reinforced concrete members is quantified from an approach proposed by Markić et al. [30], which is based on Pfyl's fibre engagement model for steel fibre reinforced concrete [31]. The Tension Chord Model [32] can be applied to textile reinforced concrete members with and without the addition of short fibres and is used to predict the load-deformation behaviour and the crack widths of the flexural members.

2. Textile reinforced concrete members with short fibres

The addition of short fibres to reinforced concrete members leads to a reduction of stresses in the reinforcement at a crack since a part of the load is transferred by fibres bridging the crack [33]. Most types of short fibres are pulled out of the matrix with increasing crack opening, which leads to a softening response for moderate and low amounts of fibres [34]. Therefore, the mechanical behaviour of strain softening fibre reinforced concrete is essentially dependent on the crack width and generally cannot be described using mean strains as in most continuous reinforcement types.

2.1. Modelling the flexural response of fibre reinforced concrete

Bending cracks typically exhibit a fairly linear opening from the crack tip to the crack mouth, which means that the concrete effective tensile stress due to the fibres (σ_{cf}, referred to in the following as effective fibre stress) is not constant over the crack length. Several approaches to estimate the behaviour of fibres for cracks opening orthogonally and skew with respect to the longitudinal reinforcement exist in the literature (e.g. [31,35,36]). The fibre activation and pull-out model by Pfyl [31] presents a mechanically based approach, which – despite its simplicity – achieves to accurately capture the global behaviour of steel fibre reinforced concrete, as shown by Markić et al. [30]. The effective fibre stress in the pull-out phase is characterised by a hyperbolic function depending on the crack opening:

$$\sigma_{cf}(u) = \sigma_{cf0}\cdot\left(1 - \frac{2\cdot u}{l_f}\right)^2 \tag{1}$$

where l_f = fibre length; u = crack opening; σ_{cf0} = fibre effectiveness, which depends on the fibre amount, slenderness and orientation, as well as on the bond between the fibre and the concrete.

However, in many cases, the post-cracking behaviour of fibre reinforced concrete is determined empirically from standardised experiments (such as direct tension [37], double punch [38] or three-point bending tests [26]) and simplified to idealised material laws (e.g. [39]).

The effective fibre stress-crack opening relationship (either determined analytically or empirically) allows formulating equilibrium at the cracked cross-section depending on the crack mouth opening (w_r), as shown in Fig. 1a. Using Eq. (1) and neglecting the tensile strength of the concrete at the crack, the resisted bending moment is

$$\begin{aligned} M = {} & \underbrace{\sigma_t\cdot A_t\cdot\left(d - \frac{x_c}{3}\right)}_{\text{textile reinforcement}} \\ & \underbrace{+ b\cdot(h - x_c)\cdot\frac{\sigma_{cf0}}{3}\cdot\left(\xi^2 - 3\cdot\xi + 3\right)\cdot\left(\frac{3\cdot\xi^2 - 8\cdot\xi + 6}{4\cdot\xi^2 - 12\cdot\xi + 12}\cdot(h - x_c) + \frac{2\cdot x_c}{3}\right)}_{\text{contribution from fibres}} \end{aligned} \tag{2}$$

where σ_t = stresses in the textile reinforcement; A_t = cross-sectional area of the textile reinforcement; d = static depth of the textile reinforcement; x_c = depth of the compression zone; h = cross-section height; and.

$$\xi = \frac{2\cdot w_r}{l_f} \tag{3}$$

Note that Eq. (2) applies for $\xi \leqslant 1$, i.e., until all fibres have been pulled out at the crack mouth. A detailed derivation of Eq. (2) can be found in the Appendix.

The total bending moment consists of the contributions from the textile reinforcement and the fibre reinforced concrete. While the effective fibre stress is dependent on the crack opening, the stresses in the textile reinforcement follow from the mean strains (ε_{tm}), which can be estimated from the average crack width and spacing (s_r) when neglecting the concrete mean tensile strains (ε_{cm}):

$$\varepsilon_{tm} = \frac{w_r}{s_r} + \varepsilon_{cm} \approx \frac{w_r}{s_r} \tag{4}$$

2.2. Prediction of the load-deformation and crack behaviour based on the Tension Chord Model

Former studies on the behaviour of weft-knitted textile reinforced concrete members in tension [19] and bending [20] concluded that the Tension Chord Model ('TCM') [32] yielded a good prediction of the global load-deformation behaviour, the stress–strain relationship of the tension chord, and the crack behaviour (crack widths and spacing). The TCM uses a stepped, rigid-perfectly plastic bond shear stress-slip relationship, which significantly simplifies solving the second-order ordinary differential equation of slipping bond [40,41]: knowing the (constant) bond shear stress, the variation of textile and concrete stresses is obtained simply by formulating equilibrium on the free-body diagrams of reinforcement and concrete (Fig. 1b). As in other models for tension stiffening, the reinforcement transfers a part of the tensile load through bond shear stresses to the concrete between two adjacent cracks (Fig. 1c), which reduces the mean strains of the tension chord (Fig. 1d).

The residual fibre stresses at the crack lead to a decrease in the maximum crack spacing, which is formulated as follows:

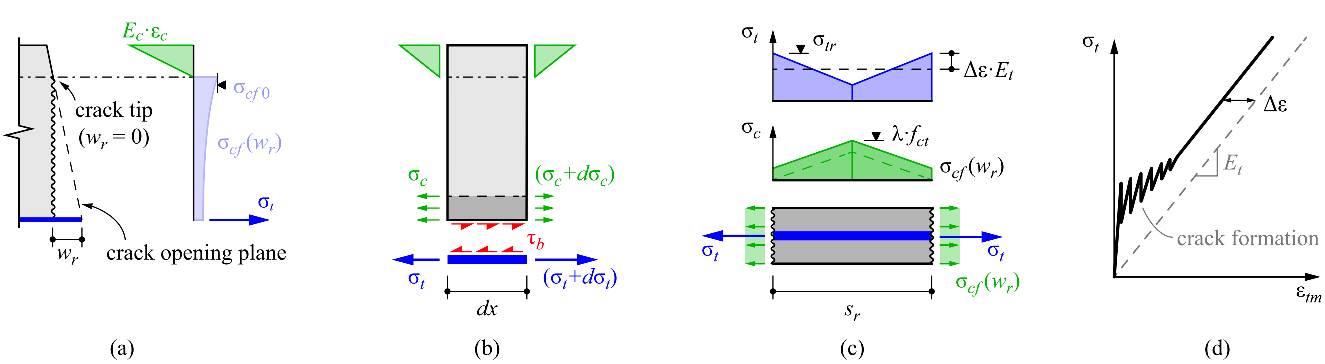

Fig. 1. Flexural response of weft-knitted textile reinforced concrete elements with short glass fibres: (a) equilibrium on cracked cross-section; (b) stress transfer between reinforcement and concrete in tension chord; (c) stresses in reinforcement and concrete following the Tension Chord Model; (d) resulting stress–strain relationship with decrease of mean strains ($\Delta\varepsilon$) due to tension stiffening.

$$s_{r0} = \frac{2 \cdot a_t \cdot f_{ct} \cdot (1 - \rho_t)}{\tau_b \cdot \rho_t} \cdot \left(1 - \frac{\sigma_{cf,cr}}{f_{ct}}\right) \tag{5}$$

where a_t = reinforcement area per unit width; f_{ct} = concrete tensile strength; ρ_t = geometrical reinforcement ratio; τ_b = bond shear stress; $\sigma_{cf,cr}$ = effective fibre stress at cracking. Note that s_{r0} corresponds to twice the transfer length required to increase the stresses in the concrete from $\sigma_{cf,cr}$ (at the crack) to f_{ct} (at the centre between cracks). The tension stiffening effect is essentially influenced by the reinforcement ratio and the effective fibre stress at cracking:

$$\Delta\varepsilon(w_r) = \frac{\lambda \cdot f_{ct} \cdot (1 - \rho_t)}{2 \cdot \rho_t \cdot E_t} \cdot \left(1 - \frac{\sigma_{cf,cr}}{f_{ct}}\right) \tag{6}$$

where E_t = Young's modulus of the textile reinforcement; λ = ratio of the actual to the maximum crack spacing, which lies between 0.5 and 1. For $s_r = s_{r0}$ (i.e. $\lambda = 1$), a new crack halving the crack spacing may form since $\sigma_c = f_{ct}$ at the centre between two cracks.

The mean strains can be obtained from the crack width and spacing using Eq. (4), neglecting the deformations in the concrete, from which the stresses in the textile reinforcement at the crack follow as:

$$\sigma_t = \varepsilon_{tm} \cdot E_t + \frac{\lambda \cdot f_{ct} \cdot (1 - \rho_t)}{2 \cdot \rho_t} \cdot \left(1 - \frac{\sigma_{cf,cr}}{f_{ct}}\right) \tag{7}$$

Setting the effective fibre stress at cracking ($\sigma_{cf,cr}$) equal to zero, the Eqs. (5), (6) and (7) yield the expressions for conventional concrete without the addition of fibres.

As already stated, the tension stiffening effect is significantly influenced by the geometrical reinforcement ratio, which is defined as the area of the reinforcement divided by the gross section of the concrete for members in uniaxial tension. For elements subjected to bending, several approaches exist for the estimation of the effective concrete area activated in tension (an overview may be found in [42]). Marti [43] and Burns [44] proposed a simple model, setting the stresses in the reinforcement of a beam at the onset of cracking equal to those of a tension chord with an equivalent reinforcement ratio at crack formation. Studies on weft-knitted textile reinforced concrete members in bending [20] showed good agreement between the predictions based on the TCM and the experimental results when using this approach. The equivalent reinforcement ratio in this study is, thus, determined from

$$\rho_{fl} = \frac{6 \cdot \alpha_{fl} \cdot A_t \cdot \left(d - \frac{x_c}{3}\right)}{h^2 \cdot b} \tag{8}$$

where $\alpha_{fl} = f_{ct}/f_{ct,fl}$ = ratio of the uniaxial to the flexural tensile strength according to *fib* Model Code 2010 [39].

3. Experimental programme

The experimental campaign consisted of 14 weft-knitted textile reinforced concrete elements tested in four-point bending. The specimens will be referred to as 'beams' in the following, although one may also refer to them as 'slab strips' due to their high slenderness. The different configurations investigated various inlay materials, fibre volumes and rib geometries. The effective fibre stress-crack opening relationship was determined from four bending tests on fibre reinforced concrete prisms (without textile reinforcement). All specimens were manufactured and tested to failure in the Structures Laboratory at ETH Zurich.

3.1. Materials and manufacturing of specimens

The dimensions of the specimens were as follows: width of 200 mm, height of 40 mm, and length of 680 mm. The weft-knitted textile reinforcement was attached to the bottom edge of the specimens (without concrete cover). However, the specimens were cast upside down, i.e. the concrete was cast first, and the reinforcement was placed on top to prevent the concrete from flowing under the reinforcement. The only exception was the reinforcement type with tall ribs, where the textile was placed at the bottom of the wooden formwork before casting. The bottom edges of these specimens had to be sealed with tape and silicon, which led to a rougher surface of the concrete near the reinforcement, making it more challenging to apply the speckle pattern for the DIC measurements, as described in Section 3.3.

3.1.1. Textiles

The textile reinforcement, which was manufactured using a CNC double bed knitting machine (Steiger Libra 3.130), was formed according to the findings from [19] and [20], which concluded that the integration of high-strength straight inlays in a base textile made from a non-structural yarn yielded the most efficient utilisation of the fibre material.

Three different materials for the inlays were examined for the specimens with fibre reinforced concrete: aramid ('AF'), carbon ('CF') and glass ('GF') fibres. The aramid and carbon fibre rovings had a fineness of 800 tex and were placed with an average spacing of 7.1 mm, whereas the glass fibres were 2400 tex at a spacing of 11.1 mm. The tensile strength and the Young's modulus of individual epoxy-coated rovings were determined in separate tension tests, as described in [19] and summarised in Table 1.

The specimens with fibre reinforced concrete had the rib layout acting as shear connectors for the bottom-edge reinforcement from the previous studies in bending, i.e. the bond ribs with an approximate height of 5 mm were made from aramid fibres with a fineness of 160 tex and only present on one side of the textile with a spacing of 40 mm (referred to as standard layout: 'ribs'), as illustrated in Fig. 2a.

The influence of four different geometries of the ribs on the bond conditions in bending was studied in specimens with aramid inlays cast with concrete without fibres. The rib geometries and layouts were variations from the already described layout used for the specimens with fibres (Fig. 2a), as illustrated in Fig. 3: (a) no ribs at all ('flat'), (b) increase of the number of ribs by 50% compared to the standard layout ('rib+'); (c) standard rib layout and introduction of transverse aramid inlays at a spacing of approximately 30 mm to strengthen the connection of the ribs to the textile ('ribX'); (d) standard rib spacing but an increase of the rib height to 30 mm ('ribT'). The inlays consisted of aramid with a fineness of 800 tex, and the ribs were made from aramid with a fineness of 160 tex.

3.1.2. Coating

The tensioned textiles were coated with a low-viscous two-component epoxy resin [45], which was applied using paint brushes. Only the inlays and the base textile were coated, while the ribs remained uncoated to allow the concrete to fill the void created by the rib, ensuring a mechanical interlock between the textile and the matrix. The epoxy coating was cured for at least 24 h at room temperature before concrete casting.

3.1.3. Concrete and short fibres

The fine-grained concrete without fibres – used for the study of the rib geometry – consisted of sand with a maximum aggregate size of 2 mm, Portland cement CEM I, micro-silica and superplasticiser at a water-to-cement ratio of 0.41 (see Table 2). The addition of short integral AR glass fibres (CEM-FIL® 62 [46], Fig. 2b) with a length of 6 mm

Table 1
Tensile strength and Young's modulus of epoxy-coated rovings from uniaxial tension tests [19].

Inlay material	f_{rov} [MPa]	E_{rov} [GPa]
Aramid	2136	116
Carbon fibre	3531	233
Glass fibre	2129	80

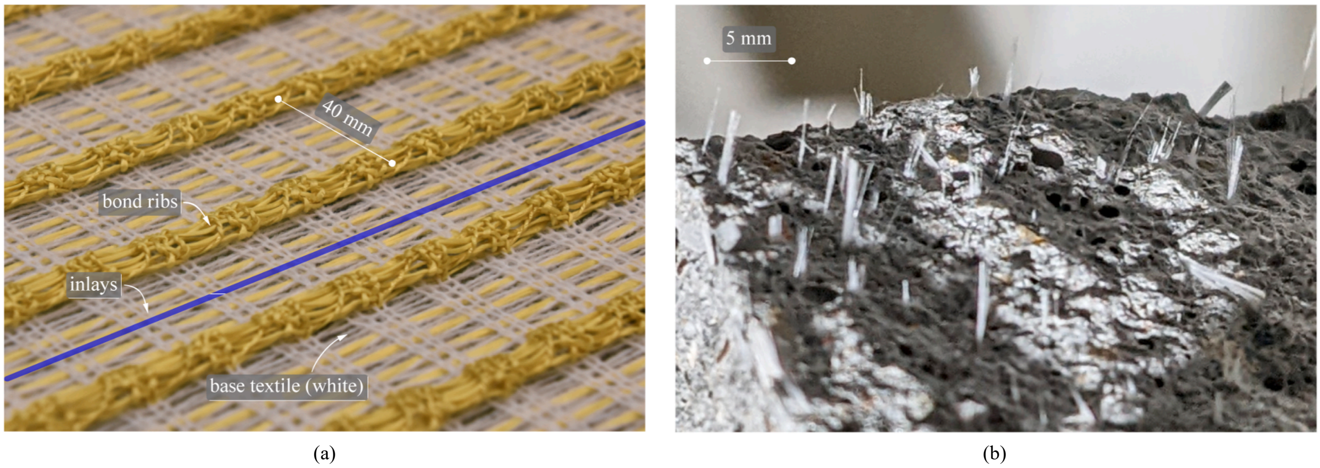

Fig. 2. Types of reinforcement: (a) weft-knitted textile reinforcement with straight inlays and standard layout of bond ribs (before casting); (b) short integral AR glass fibres in the concrete matrix (at crack face after testing).

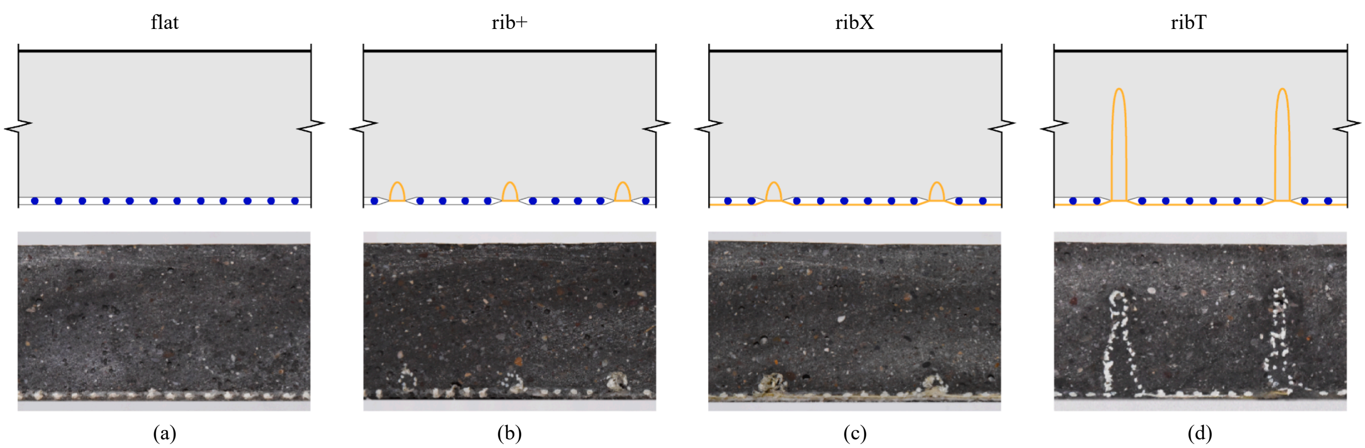

Fig. 3. Rib geometries and layouts in specimens with concrete without fibres: (a) textile without ribs ('flat'); (b) increase of rib numbers by 50% compared to standard layout ('rib+'); (c) transverse inlays at a spacing of 30 mm ('ribX'); (d) increase of rib height to 30 mm and transverse inlays ('ribT').

Table 2
Composition of concrete mixes with and without short glass fibres, and concrete material properties (mean ± standard deviation) according to EN 196–1 [47] and *fib* Model Code 2010 [39].

Fibre volume [%]	Sand (0–2 mm) [kg/m^3]	Cement [kg/m^3]	Micro-silica [kg/m^3]	Superplasticiser [kg/m^3]	Water [kg/m^3]	AR glass fibres [kg/m^3]	$f_{c,cube}$ [MPa]	$f_{ct,fl}$ [MPa]	f_{ct} [MPa]	E_c [GPa]
0	1368	616	53.6	2.92	254	0	82.5 ± 2.0	6.9 ± 0.7	3.1	24.2 ± 2.3
0.5	1355	616	53.6	3.84	254	13.5	83.0 ± 3.4	10.2 ± 1.8	4.5	24.5 ± 1.3

and a fineness of 45 tex (corresponding to a diameter of ca. 0.15 mm) at a fibre volume content of 0.5% required a slight adjustment of the amount of sand and superplasticiser in the concrete mix to maintain similar rheological properties (as summarised in Table 2). The fibres were added to the wet concrete during mixing in the laboratory. The specimens were cured in a climate chamber (25 °C and 90% relative humidity) for eight (fibre reinforced concrete) and 11 days (normal concrete) before testing.

The compressive ($f_{c,cube}$) and flexural strength ($f_{ct,fl}$) of the hardened concrete were determined according to EN 196–1 [47] on prisms of 40 mm × 40 mm × 160 mm (six prisms per batch) on the same day of the testing of the textile reinforced specimens and are summarised in Table 2. The uniaxial tensile strength (f_{ct}) was determined following the conversion formula according to *fib* Model Code 2010 [39]. The post-cracking behaviour of the fibre reinforced concrete mix was characterised by means of four bending tests on beams with the same geometry as the weft-knitted textile reinforced concrete specimens (see Section 3.2) to properly capture potential fibre orientation effects. The results of the characterisation of the effective fibre stress-crack opening relationship of fibre reinforced concrete is given in Section 4.1.

3.2. Test setup and specimens

All specimens with weft-knitted textile reinforcement were tested in four-point bending using a Walter + Bai 100 kN universal testing machine. The total span was 500 mm with shear spans of 140 mm, resulting in a constant moment zone with a length of 220 mm, as shown in Fig. 4. Table 3 summarises all configurations of the weft-knitted textile reinforced concrete beams and their geometrical parameters. The fibre reinforced concrete beams for material characteristation were tested in three- and four-point bending (two specimens each) with the same geometry as the weft-knitted textile reinforced specimens, as already

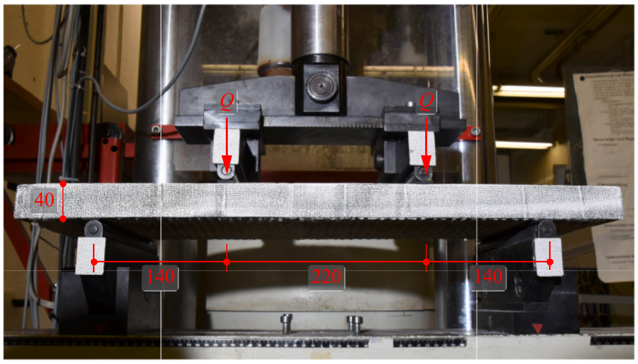

Fig. 4. Setup and dimensions of four-point bending test (dimensions in [mm]).

mentioned in Section 3.1.3, but without constant moment zone in case of the three-point bending test.

The supports and the load introduction consisted of cylindrical rollers (see Fig. 4), allowing the free rotation and horizontal elongation of the specimens. The tests were run with a controlled displacement rate of the hydraulic actuator, which was varied as follows:

- Before cracking: 0.2 mm/min
- Crack formation phase: 0.5 mm/min
- Stabilised cracking phase: 1.0 mm/min

3.3. Instrumentation

The force measurements were taken from the load cell installed in the testing machine. The bending moment was calculated by multiplying the applied load by the shear span. The deformations were measured using 3D digital image correlation (DIC). One side of the specimen was painted white and speckled with a black random pattern with a speckle size of 0.7 mm to increase the contrast, thus improving the correlation. Two high-resolution cameras (FLIR Grasshopper®3, 4096 × 3000 px) with lenses of 25 mm focal length (Linos MeVis-C) were installed at a stereo angle of approximately 25°. The field of view covered the beam on a length of approximately 585 mm and exhibited an average resolution of 7.0 px/mm. The correlation was carried out using the commercial software 'VIC-3D' (Correlated Solutions Inc. [48]), using the following parameters: subset size = 19 px; step size = 5 px; strain filter size = 9. The zero displacement test according to [49] and [50] resulted in an average noise level of $\sigma(U,V) = 0.8 \cdot 10^{-6}$m and $\sigma(\varepsilon_1, \varepsilon_2) = 80\ \mu\varepsilon$.

The quasi-continuous displacement and strain fields from the digital image correlation measurement were analysed with the open-source software ACDM [51,52], yielding the crack patterns and the crack widths. The DIC measurements could not directly assess the deformations at the bottom edge of the specimens due to the subset size limiting the correlated area of interest, as described in [20]. Therefore, the crack widths at the depth of the reinforcement (crack mouth opening) were extrapolated from the measured crack widths by assuming linearly opening cracks.

4. Results and discussion

The results of the fibre reinforced concrete experiments and the weft-knitted textile reinforced concrete experiments are analysed in the following to investigate the load-deformation behaviour and failure modes. The measurements from digital image correlation allow a detailed consideration of the crack behaviour for all specimens and the deformations in the tension chord for the specimens with continuous reinforcement. The fibre reinforced concrete specimens without weft-knitted textile are analysed in Section 4.1 to characterise the effective fibre stress-crack opening relationship. This relationship is then applied in Section 4.2 to assess the stresses at the cross-section in the flexural response of the specimens with both short fibres and continuous textile reinforcement, following the approach described in Section 2.1. The influence of various rib geometries on the flexural behaviour of weft-knitted textile reinforced concrete experiments without fibres is analysed in Section 4.3. The experimental results are compared in Sections 4.2.4 and 4.3.2 to the predictions following the Tension Chord Model for specimens with and without short fibres, respectively.

4.1. Characterisation of the effective fibre stress-crack opening relationship of glass fibre reinforced concrete

The contribution of the short fibres to the load-bearing behaviour can be characterised by an equivalent effective fibre stress-crack opening relationship, as described in Section 2.1. In this study, the hyperbolic function following Pfyl's fibre engagement model for steel fibres (Eq. (1)) is adopted. However, the pull-out behaviour of integral short glass fibres is presumably different to the one of hooked steel fibres, and the resistance of a single short glass fibre pulled out from a matrix exhibits large scatter due to various failure types such as fibre breakage at the crack edges or partial pull-out of the filament core from the fibre sleeve as observed in [22]. Therefore, the fibre effectiveness (σ_{cf0}) and the activated fibre length (l_f) in Eq. (1) were calibrated experimentally from four glass fibre reinforced concrete beams in three- and four-point bending. All specimens tested for material characterisation exhibited the formation of a single crack where the deformations concentrated,

Table 3
Specimen configuration of weft-knitted textile reinforced concrete beams with various fibre materials, rib geometries and short glass fibre volume content (A_t = cross-section area of the textile reinforcement; ρ_{fl} = equivalent geometrical reinforcement ratio in bending; b = width of the specimen; d = depth of the reinforcement; V_f = volumetric fibre content).

Specimen	Inlay material	Rib layout	No. of inlays	A_t	ρ_{fl}	b	d	V_f
			[-]	[mm^2]	[%]	[mm]	[mm]	[%]
AF-fib	Aramid	ribs	30	16.7	0.54	201.7	38.6	0.5
			30	16.7	0.52	202.0	39.9	
CF-fib	Carbon fibre	ribs	29	13.2	0.42	200.9	38.7	
			30	13.6	0.43	200.8	39.4	
GF-fib	Glass fibre	ribs	20	18.8	0.60	201.4	38.1	
			20	18.8	0.60	200.8	38.3	
AF-flat	Aramid	flat	39	21.7	0.68	202.0	39.4	0.0
			40	22.2	0.71	202.3	37.9	
AF-rib+		rib+	30	16.7	0.53	201.9	39.1	
			30	16.7	0.49	202.4	42.0	
AF-ribX		ribX	28	15.6	0.50	201.2	38.3	
			30	16.7	0.52	201.0	37.9	
AF-ribT		ribT	30	16.7	0.60	193.4	35.9	
			30	16.7	0.59	193.3	37.1	

resulting in a deflection softening response. The crack mouth opening (CMO) was determined from the DIC measurements and the analysis using ACDM. Linear regression was applied on the crack opening to obtain the crack width at the bottom edge of the specimen, where no direct measurements from DIC were available. Fig. 5a shows the moment-crack opening relationship for all tested specimens (grey lines). The residual effective fibre stresses obtained from the four-point bending tests were slightly lower than in the three-point bending tests, given that the crack location was not predefined and the crack formed in the weakest section. However, the differences were small and the results show fairly low scatter, which indicates a uniform distribution of the fibres within the concrete elements. The beams with combined continuous textile and short fibre reinforcement typically exhibited multiple evenly distributed cracks and a fairly linear load increase with increasing deformations (as described in 4.2), which means that not all cracks necessarily formed at the weakest section. Therefore, the results from both the three- and four-point bending tests were used to calibrate the parameters in Pfyl's fibre engagement model.

The parameters σ_{cf0} and l_f from Eqs. (2) and (3) (neglecting the depth of the compression zone) were calibrated based on the experimental data using the least-squares method, which yielded $\sigma_{cf0} = 1.67$ MPa and $l_f = 1.03$ mm. The calibrated fibre length is considerably smaller than the actual length of the glass fibres used in the mix. The visual inspection of the broken specimens showed that – although some fibres maintained their integral form, as illustrated in Fig. 6a – in many cases, individual filaments disbanded from the fibre and some even broke prematurely (see Fig. 6b), which considerably decreased the pull-out resistance of the fibres.

The moment-crack mouth opening relationship corresponding to the calibrated parameters is represented as red line in Fig. 5a. The equivalent fibre stress-crack opening relationship could then be obtained from Eq. (1), as shown in Fig. 5b. The distribution of the fibre stresses over the cross-section for various crack mouth openings, neglecting the depth of the compression zone, is shown in Fig. 5c. Note that the expressions from Eqs. (1) and (2) are only valid for $w_r \leqslant l_f/2$, but all experimental crack openings analysed in the following stayed within this limit.

4.2. Flexural response of weft-knitted textile reinforced concrete with short fibres

This section presents the load-deformation and crack behaviour of the weft-knitted textile reinforced concrete beams with short fibres. For

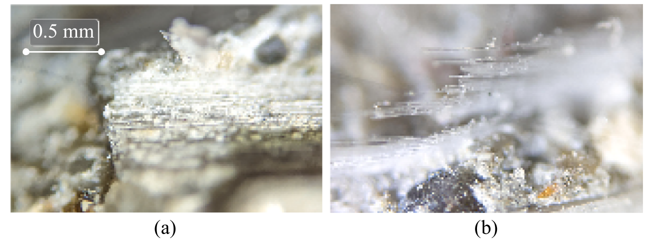

Fig. 6. Short glass fibres at broken crack face: (a) integral fibre end; (b) separated filaments.

assessing the mean strains in the tension chord, the measurements from digital image correlation were downsampled to two rows of data. Following the methodology described in [20], the linear regression on the horizontal deformations of the lower row of data points and the assumption of plane sections remaining plane yielded the mean strains at the depth of the reinforcement within the constant moment zone. The stresses in the textile reinforcement were determined from Eq. (2), applying the effective fibre stress-crack opening relationship calibrated in Section 4.1 and the crack mouth opening and the depth of the compression zone within the constant moment zone determined from the crack analysis using ACDM and assuming linearly opening cracks, as described in [20]. The contributions from the continuous textile reinforcement and the short fibres to the total bending moment were determined using Eq. (2).

4.2.1. General behaviour and failure modes

The load-deformation behaviour of the reinforced concrete beams, shown in Fig. 7, generally followed the typical response known from textile reinforcement as it was mainly governed by (i) the uncracked state, (ii) the crack formation and (iii) the stabilised cracking phase. While the moment-deflection relationship (Fig. 7) exhibited a fairly linear post-cracking behaviour, most specimens exhibited a decrease of flexural stiffness near the ultimate load. In some cases, the applied load displayed a significant drop before increasing again, with the eventual collapse occurring at approximately the initially reached load (Specimen 'GF-fib-2' even exceeded the former). The reasons for this behaviour are discussed in more detail at the end of this section.

Several evenly distributed cracks formed within the constant moment zone in all specimens shortly after initial cracking, as illustrated by the crack patterns in Fig. 8, where the line thicknesses are

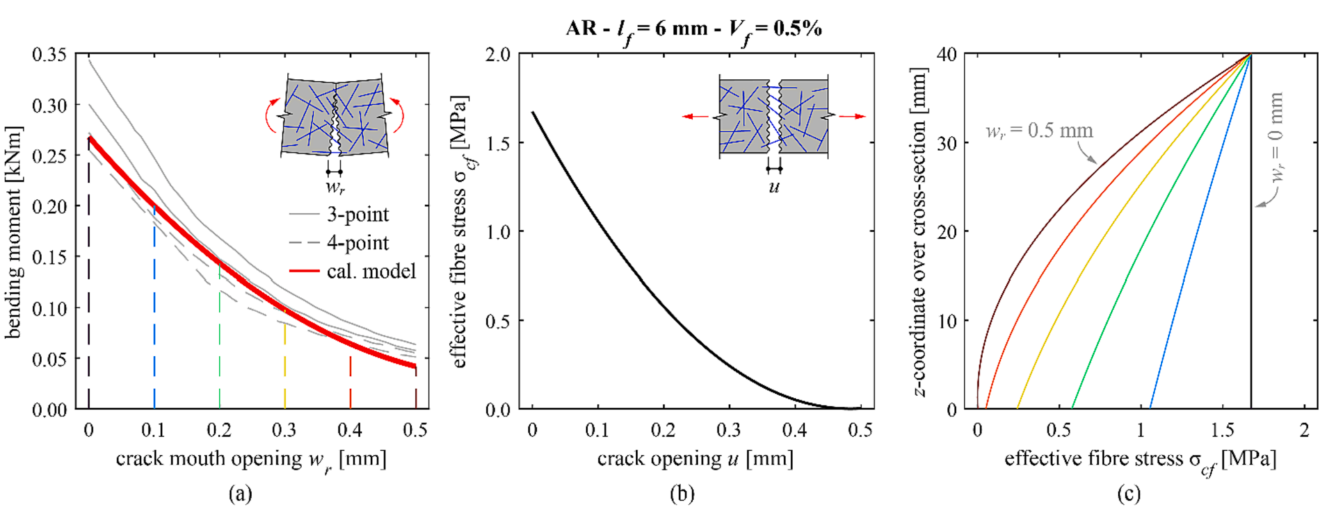

Fig. 5. Mechanical characterisation of glass fibre reinforced concrete: (a) bending moment-crack mouth opening relationship from material characterisation tests (grey) and calibrated model (red); (b) effective fibre stress-crack opening relationship calibrated on experimental results; (c) equivalent fibre stress distribution over the cross-section for various crack mouth openings using the calibrated model (neglecting the depth of the compression zone). (For interpretation of the references to colour in this figure legend, the reader is referred to the web version of this article.)

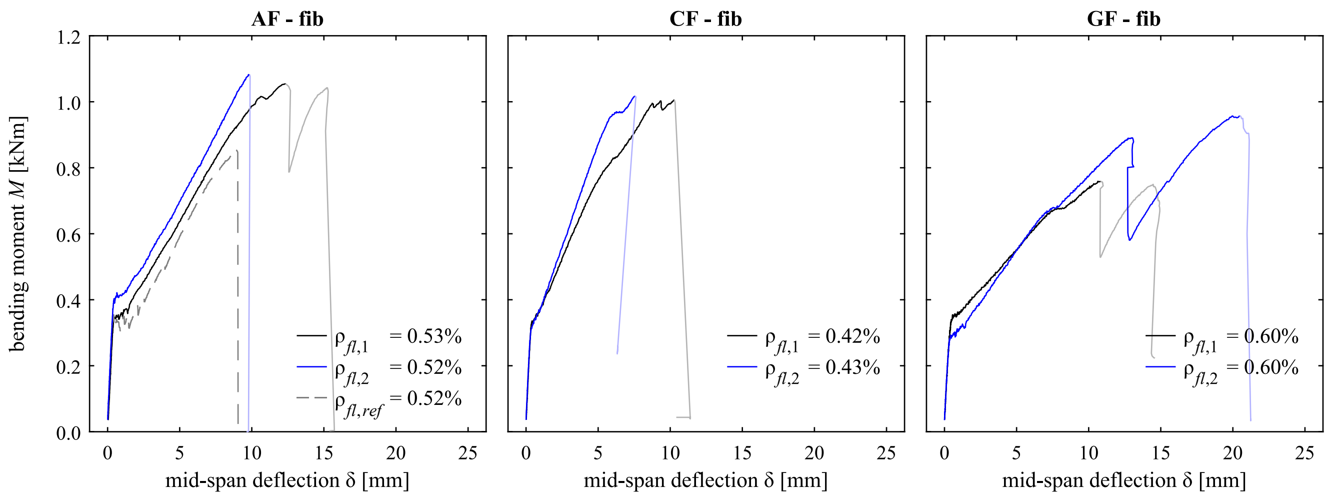

Fig. 7. Moment-deflection relationship of weft-knitted textile reinforced concrete beams with short integral glass fibres (solid lines) and reference test for specimen with aramid inlays and concrete without fibres (dashed).

proportional to the crack widths just before failure and the governing crack is marked in red, with its normalised displacement vector in grey and rose lines. All specimens displayed a brittle failure mode at relatively low utilisation levels of the textile reinforcement (σ_{tu}/f_{rov} = 0.48 ÷ 0.76, as summarised in Table 4). In most cases, a shear crack formed just outside the constant moment zone, as illustrated in Fig. 8, and the eventual failure occurred due to the delamination of the reinforcement from the concrete (Fig. 9a). Thereby, the bond ribs stuck to the concrete as the textile broke at the connection between the ribs and the base fabric with the inlays, as shown in Fig. 9b. The linear opening of the governing crack in Specimen 'CF-fib-1' (Fig. 8) suggests a more bending-like failure. However, the low utilisation of the textile reinforcement and the visual inspection of the specimen after testing revealed that the inlays had not ruptured, but the reinforcement had delaminated over the whole shear span to the end anchorage, as shown in Fig. 9c.

Some specimens ('AF-fib-1', 'GF-fib-1' and 'GF-fib-2') exhibited two shear cracks on both sides of the span. The formation of the first shear crack led to the sudden drop of the applied force and a substantial opening of the crack. However, the reinforcement did not fully debond, although a delamination crack along the reinforcement in the shear span started visibly forming, as shown in Fig. 9d. The applied load increased again to approximately the formerly attained peak load, and the specimen eventually collapsed due to the delamination of the reinforcement in a new shear crack on the opposite side of the span. The geometry of the shear cracks may have led to a mechanical interlock of the crack edges, as can be seen in Fig. 8 and Fig. 9d. Despite the large crack openings in the upper and lower part of the shear crack, the middle section stayed in contact but subjected to a large slip, resulting in stresses due to aggregate interlock and friction bridging the crack until the collapse in the governing shear crack in the opposite span occurred.

4.2.2. *Contribution of short integral glass fibres to the load bearing behaviour*

The contributions from the textile reinforcement and the effective concrete tensile stress offered by the fibres were determined from Eq. (2) and are illustrated in Fig. 10, where the maximum crack mouth opening within the constant moment zone at every load step and the corresponding depth of the compression zone were considered to estimate the equivalent effective fibre stresses.

The influence of the fibres on the bending behaviour was mainly relevant for the behaviour in the serviceability limit state (Fig. 10). While the contribution from the fibres governed the response just after cracking, the contribution of the textile reinforcement successively increased due to the steep decrease of the effective fibre stress (see Eq. (1) and Fig. 5) and the increase of textile stresses for larger crack widths

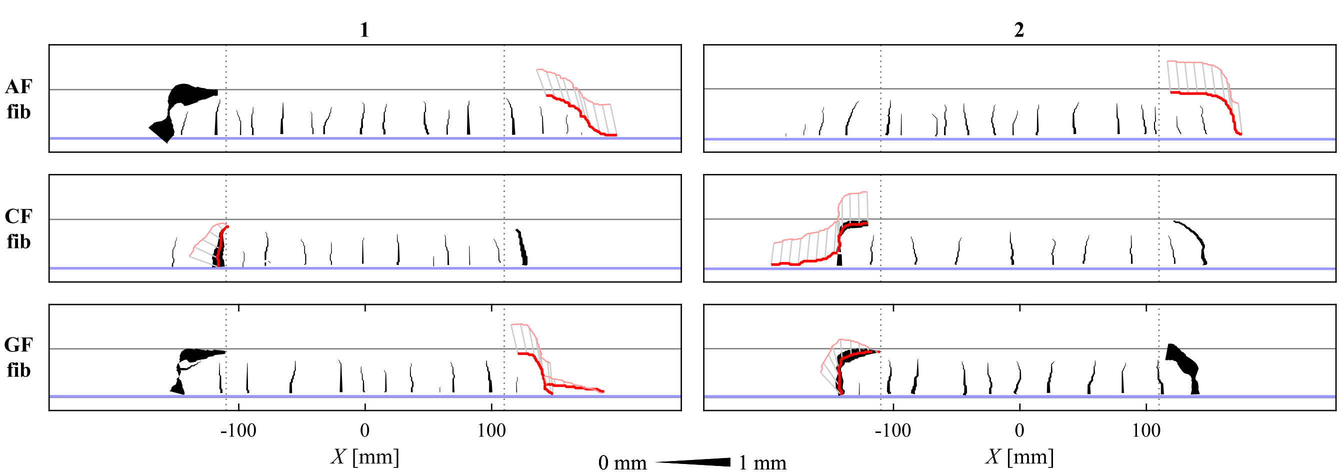

Fig. 8. Crack patterns shortly before failure for weft-knitted textile reinforced concrete beams with short integral glass fibres (thickness of contours corresponding to crack width; governing crack marked in red with normalised displacement vector in grey and rose lines). (For interpretation of the references to colour in this figure legend, the reader is referred to the web version of this article.)

Table 4
Textile stresses at ultimate load (σ_{tu}), utilisation of textiles compared to roving strength (f_{rov}), measured Young's modulus ($E_{t,meas}$), bond shear stresses (τ_b) back-calculated from uniaxial tension tests [19], and comparisons of measured crack widths ($w_{r,meas}$) and spacings ($s_{r,meas}$) with predictions using the Tension Chord Model ($w_{r,TCM}$, $s_{r,TCM}$) at various load levels.

Specimen	σ_{tu} [MPa]	σ_{tu}/f_{rov} [-]	$E_{t,meas}$ [GPa]	τ_b [MPa]	at 0.5 × σ_{tu}: $w_{r,meas}$ [mm]	at 0.5 × σ_{tu}: $w_{r,TCM}$ [mm]	at 1.0 × σ_{tu}: $w_{r,meas}$ [mm]	at 1.0 × σ_{tu}: $w_{r,TCM}$ [mm]	$s_{r,meas}$ [mm]	$s_{r,TCM}$ [mm]
AF-fib	1618	0.76	131.1	2.0	0.11	0.09 ÷ 0.14	0.26	0.27 ÷ 0.49	22.5	20.9 ÷ 41.8
	1592	0.75	126.5		0.09	0.09 ÷ 0.13	0.24	0.27 ÷ 0.49	21.2	21.6 ÷ 43.2
CF-fib	1854	0.53	211.3	1.3	0.09	0.08 ÷ 0.11	0.17	0.23 ÷ 0.42	21.6	32.4 ÷ 64.8
	1837	0.52	251.2		0.08	0.08 ÷ 0.11	0.21	0.24 ÷ 0.43	30.3	33.0 ÷ 66.0
GF-fib	1017	0.48	86.9	1.9	0.06	0.05 ÷ 0.05	0.26	0.24 ÷ 0.42	26.7	21.2 ÷ 42.4
	1332	0.63	91.9		0.13	0.10 ÷ 0.15	0.38	0.33 ÷ 0.59	28.3	21.3 ÷ 42.7
AF-flat	943	0.44	33.1	2.0	0.10	0.10 ÷ 0.10	1.11	0.24 ÷ 0.39	87.5	34.1 ÷ 68.2
	862	0.40	83.6		0.03	0.10 ÷ 0.11	0.14	0.23 ÷ 0.38	21.6	32.8 ÷ 65.6
AF-rib+	1591	0.74	109.6		0.12	0.12 ÷ 0.19	0.27	0.28 ÷ 0.50	23.6	22.8 ÷ 45.6
	1560	0.73	118.5		0.12	0.13 ÷ 0.20	0.31	0.30 ÷ 0.53	29.6	24.5 ÷ 49.0
AF-ribX	1537	0.72	119.3		0.11	0.12 ÷ 0.18	0.25	0.27 ÷ 0.48	23.4	22.3 ÷ 44.6
	1721	0.81	122.1		0.13	0.14 ÷ 0.22	0.26	0.30 ÷ 0.55	21.3	22.1 ÷ 44.2
AF-ribT	2638	1.24	129.4		0.18	0.22 ÷ 0.39	0.34	0.45 ÷ 0.86	18.0	20.9 ÷ 41.8
	2370	1.11	132.4		0.13	0.20 ÷ 0.35	0.29	0.42 ÷ 0.79	18.1	21.6 ÷ 43.2

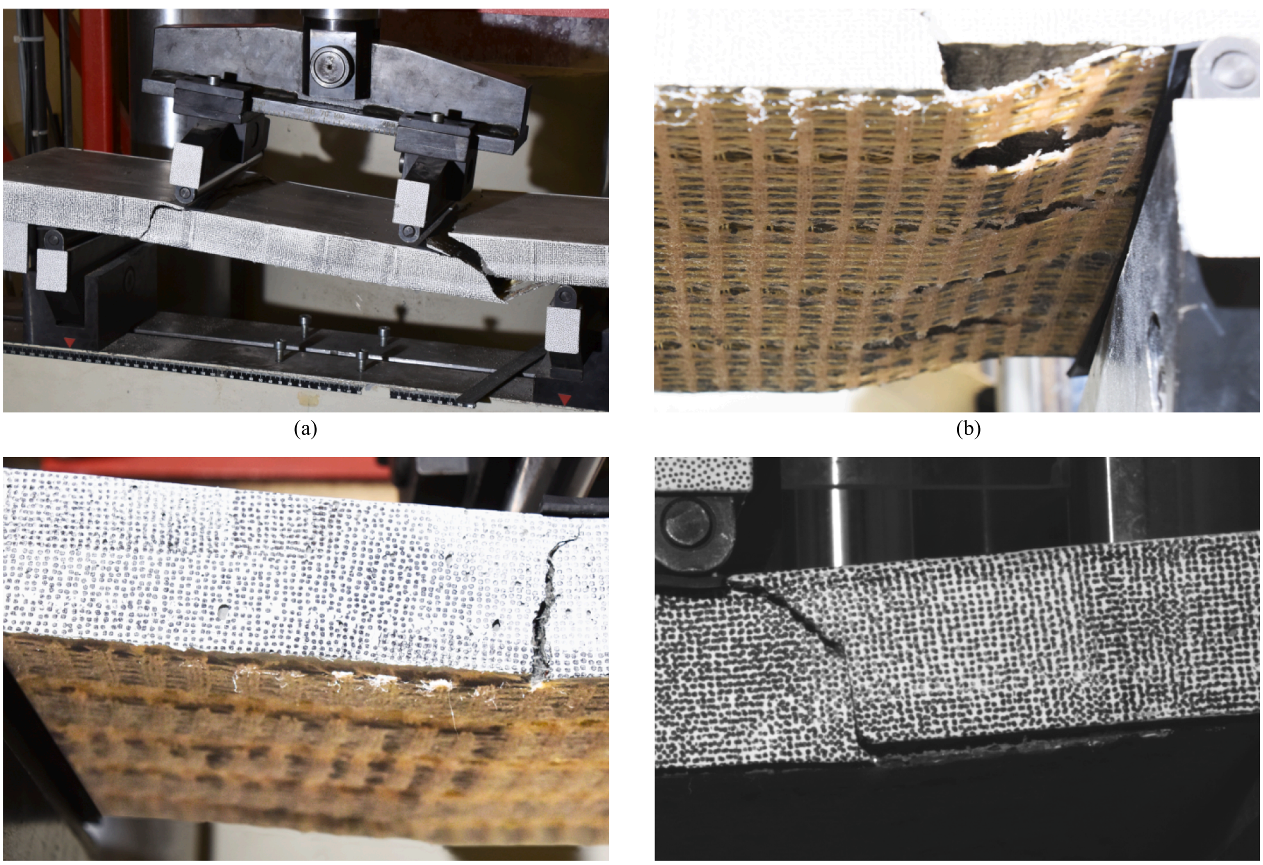

(a) (b) (c) (d)

Fig. 9. Failure modes of weft-knitted textile reinforced concrete specimens with short fibres: (a) shear crack with delamination of reinforcement ('AF-fib-1'); (b) rupture of connection between bond ribs and base textile with the inlays ('AF-fib-2'); (c) delamination of reinforcement due to bending crack ('CF-fib-1'); (d) delamination of reinforcement in a secondary shear crack ('GF-fib-2').

(following Eqs. (2) and (4)), as illustrated in Fig. 10d. Since all specimens failed prematurely before reaching the bending resistance, the textile stresses were well below the roving strength, and the contribution from the short fibres to the bending moment might be potentially negligible at the expected crack widths when reaching the full capacity of the textile reinforcement.

Regarding the contribution of the fibres to the shear resistance of the beam, most of the governing cracks exhibited a steep shape with a nearly horizontal crack branch at the upper edge of the specimen. The short fibres in the concrete are expected to exhibit rather low effectiveness under such loading conditions due to the foremost slipping motion at failure and the consequently wide pull-out angle (close to parallel to the crack edge) [53], and the potential horizontal alignment of the fibres close to the specimen edge [54] (with the fibres being oriented nearly parallel to the horizontal crack branch). Furthermore, the effective fibre stress obtained from the FRC specimens, as described in Section 4.1,

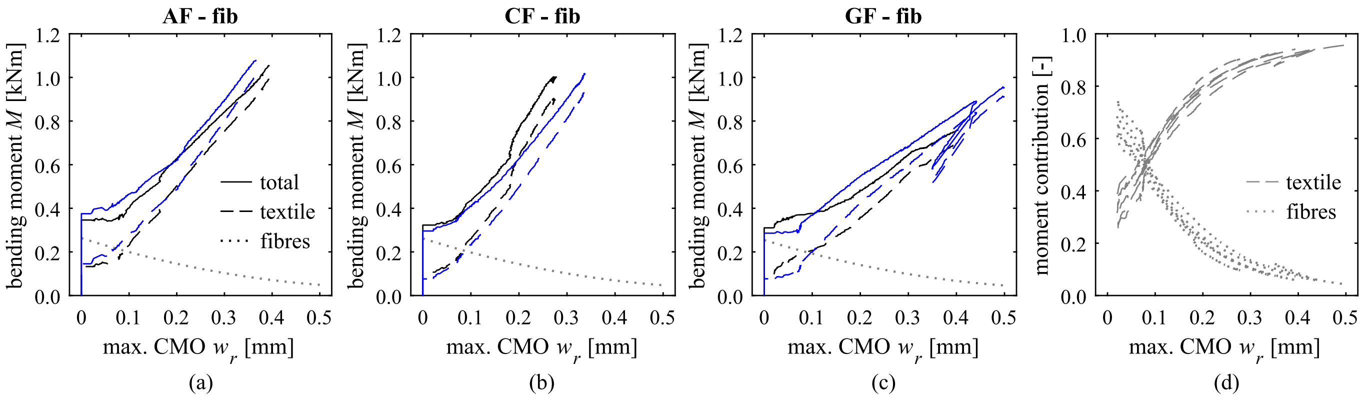

Fig. 10. Contributions from textile and fibre reinforcement to bending moment resistance: specimens with (a) aramid, (b) carbon fibre, and (c) glass fibre inlays; (d) relative contributions to total bending moment.

suggests that the contribution from the fibres to the shear transfer may be negligible due to the large crack widths observed in the governing crack before failure. The specimens with aramid inlays still reached higher peak loads when compared to the reference specimen without short fibres (dashed line in Fig. 7), but the failure mode was essentially the same. However, such variations in the shear resistance are – although most configurations exhibited good repeatability of the results – not completely surprising as shown in the specimens with glass fibre inlays ('GF-fib').

The less pronounced effect of the short fibres in the present study compared to conventional textile reinforcement, especially regarding the beneficial effect on the bond conditions as documented in the literature (e.g. [23,24,55]), can be explained by the specific geometries of weft-knitted and woven textiles. Conventional textile reinforcement

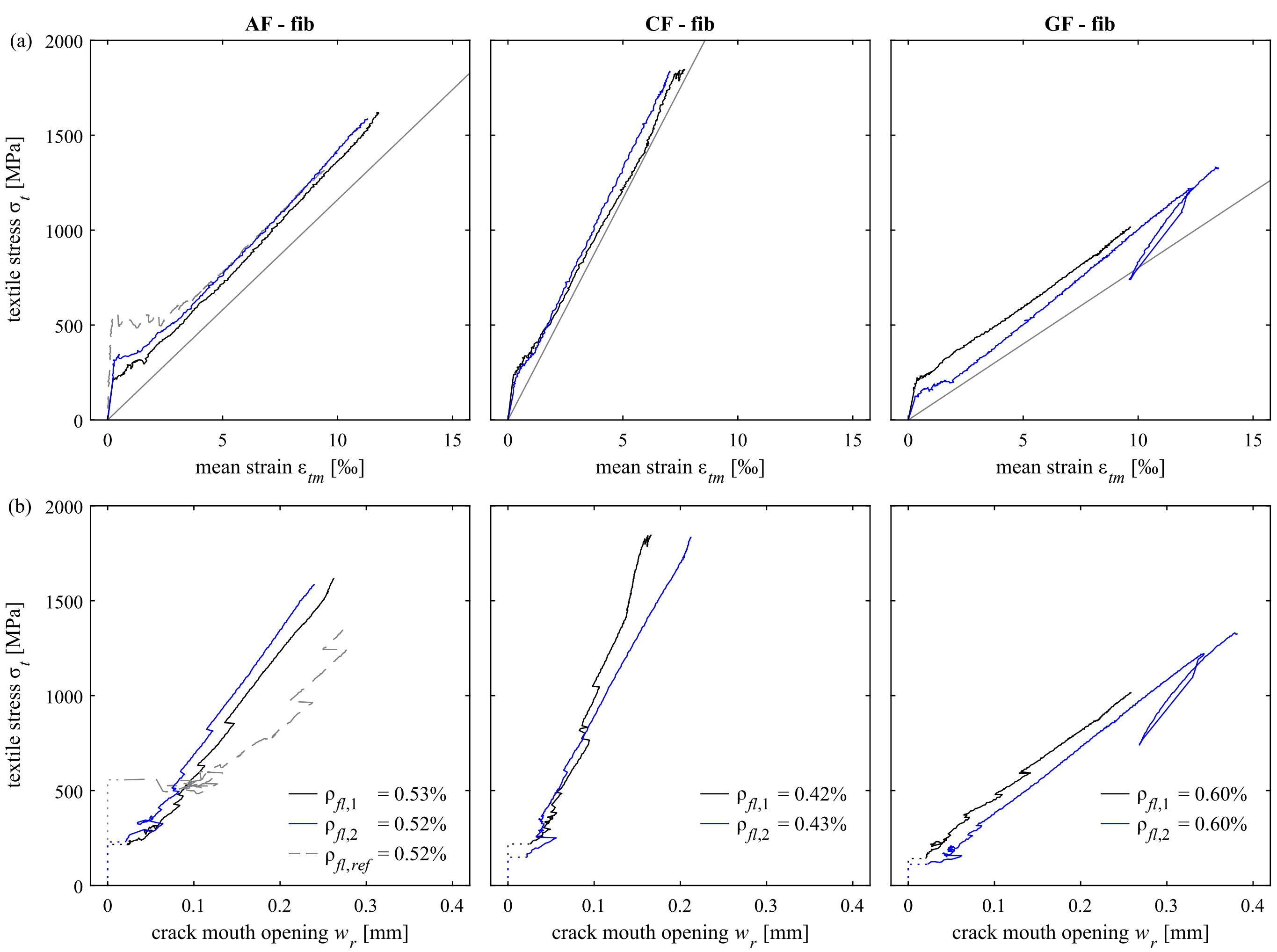

Fig. 11. Mechanical behaviour of weft-knitted textile reinforced concrete beams with short integral glass fibres (solid lines) and reference test for specimen with aramid inlays and normal concrete (dashed) from [20] – experimental results and predictions using the Tension Chord Model [32] (TCM, denoted as grey area): (a) textile stress vs mean strain in the tension chord within the constant moment zone; (b) textile stress vs crack mouth opening in the constant moment zone.

typically consists of an orthogonal grid of straight textile rovings with a certain spacing, which allows the concrete to flow through the reinforcement layer, enclosing the individual strands. The addition of short fibres to the concrete thus increases the delamination and splitting resistance since the fibres bridge the cracks initiated by the presence of the textile reinforcement. On the other hand, weft-knitted textiles intended for the use as flexible formworks exhibit a closed surface where the bond conditions rely on adhesion, friction and the mechanical interlock between concrete and potential spatial features. Therefore, the short fibres do not directly influence the interface conditions between textile and concrete, but may only improve the behaviour of cracks formed within the concrete matrix.

4.2.3. Response of the tension chord and crack behaviour

The stress–strain and the stress-average crack width relationships of the tension chord within the constant moment zone (Fig. 11a-b) stayed fairly linear up to failure. The Young's moduli were determined in the range of 60% to 80% of the ultimate load (ensuring that cracking had stabilised for all specimens, but before peculiar effects near failure may have influenced the behaviour) using linear regression and are summarised in Table 4; the stiffness of the textile reinforcement generally corresponded well with the roving tests (represented as grey lines in Fig. 11a). Specimen 'GF-fib-2' experienced an uncontrolled unloading after reaching the first local load peak but exhibited a similar load-deformation behaviour during the subsequent load increase as the stress–strain relationship and the average crack width measurements returned to the original behaviour once the formerly reached load had been exceeded. Some specimens – most distinctively observed in 'CF-fib-1' – displayed a distinct increase in stiffness ('kink') close to failure, which is also represented in the measurements of the average crack width within the constant moment zone (Fig. 11b). This phenomenon can be explained by analysing the crack kinematics. In most specimens, the majority of bending cracks formed shortly after the concrete reached its tensile strength, leading to an early stabilisation of the crack pattern and a fairly linear increase of the average crack width with the textile stress. The few additional cracks in the constant moment zone that formed in the cracked-elastic phase did not significantly affect the global load-deformation behaviour but are visible as small steps in the average crack width measurements (e.g. 'AF-fib-1' or 'GF-fib-1').

In Specimen 'CF-fib-1', one bending crack exhibited a significantly larger crack width than all other cracks, as illustrated in Fig. 8. Since it had formed just outside the constant moment zone, it was neither accounted for in the assessment of the mean strains in the tension chord nor the average crack width measurements. Consider now Fig. 12, which shows the crack mouth opening against the utilisation of the textile reinforcement (i.e. textile stress divided by the roving strength) for all cracks within the constant moment zone (in grey), the governing crack (in red), and secondary shear cracks that, however, did not eventually lead to failure (in blue). The average crack width value of the cracks within the constant moment zone is shown in black. Compared to most other specimens, the deformations in 'CF-fib-1' started concentrating in the governing crack considerably before reaching the ultimate load, which led to the stagnation in the cracks within the constant moment zone, reflected by the apparent stiffness increase in Fig. 11a. Other specimens such as 'AF-fib-1' or 'GF-fib-1' displayed a similar behaviour, where the deformations concentrated in a secondary shear crack close to

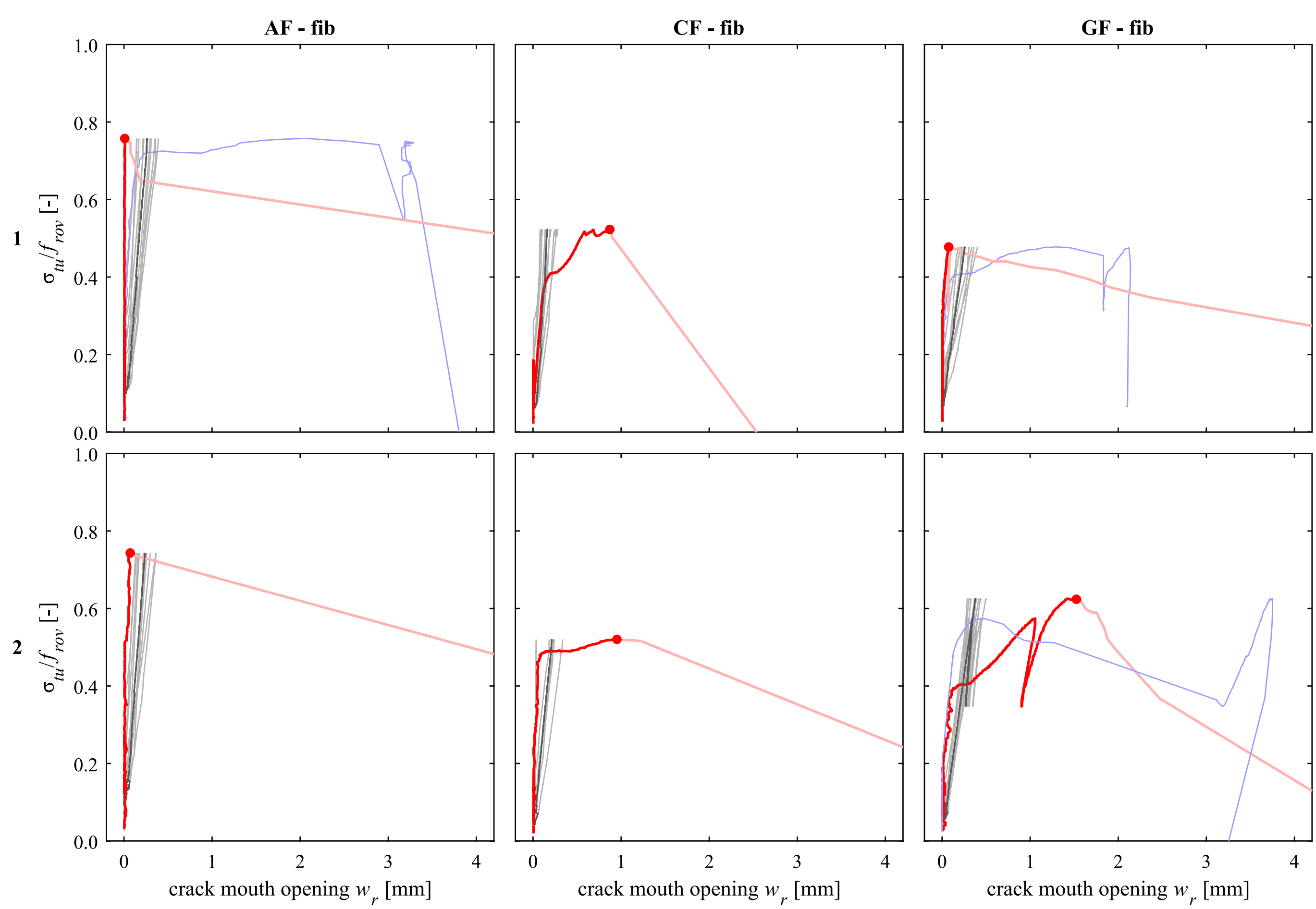

Fig. 12. Crack mouth openings of all cracks within the constant moment zone (grey; average crack width in black), and average crack opening of secondary shear cracks (blue) and governing crack (red, with circle denoting the peak load) for all specimens with short integral glass fibres. (For interpretation of the references to colour in this figure legend, the reader is referred to the web version of this article.)

the ultimate load. In these cases, this effect was visible as a decrease in the flexural stiffness in the moment-deflection relationships but was less pronounced in the stress–strain curves and crack width measurements. These observations highlight that the methodology to assess the deformations in the tension chord, as described in [20], is particularly suitable for specimens with evenly distributed and uniformly opening bending cracks within the constant moment zone, which was the case for all specimens in the serviceability limit state. However, the results need to be treated more cautiously once deformations start concentrating in a single crack or shear cracks form.

The effect of the short fibres was mostly visible in the observed crack mouth openings (Fig. 11b): the reference specimen exhibited considerably wider cracks due to the larger crack spacing ($s_{r,meas}$ = 28.1 mm) compared to the specimens with fibre reinforced concrete ($s_{r,meas}$ = {22.5; 21.5} mm). The stress–strain behaviour was mainly influenced during the crack formation phase, while the contribution from the short fibres continuously decreased with increasing crack mouth opening, as described in Section 4.2.2.

4.2.4. Predictions using the tension chord Model

The Tension Chord Model ('TCM'), as described in Section 2.2, was used to predict the load-deformation and crack behaviour of the textile-reinforced concrete beams with short fibres. The material parameters were determined in separate tests a priori, as described in Section 3.1. The bond shear stresses (τ_b) were obtained from an experimental study on tension ties with the same type of reinforcement [19] using the TCM. The concrete effective tensile stresses due to the fibres were obtained from the fibre reinforced concrete beams, as outlined in Section 4.1.

The predictions from the TCM are denoted as grey areas in the stress–strain relationships (Fig. 11a) and the average crack width measurements (Fig. 11b), indicating the range of results between the theoretical minimum and maximum crack spacing (i.e. λ = 0.5…1.0). The TCM correlated well with the experimental results regarding the stress–strain relationship. The tension stiffening effect in Specimen 'CF-fib-1' was slightly overestimated due to the lower Young's modulus measured in the experiments. The estimation of the crack spacings (Table 4) and the textile stress-crack width relationship (Fig. 11b) following Eqs. (5) and (7) were in a reasonable range, with the experimental results lying at the lower ends of the predictions.

4.3. Influence of various rib geometries

The evaluation of the experimental results of the textile reinforced concrete beams with various rib geometries followed the same procedure as used for the specimens with fibre reinforced concrete, described in Section 4.2. Due to the absence of short fibres, the calculation of the textile stresses from the bending moment using Eq. (2) is considerably simpler, as they can be determined directly from equilibrium at the cracked cross-section and are independent of the crack width.

4.3.1. General behaviour and failure modes

The general behaviour of the specimens with various rib geometries was similar to the beams with fibre reinforced concrete described in Section 4.2. The moment-deflection relationships in Fig. 13 show that most of the specimens with bond ribs ('rib+', 'ribX' and 'ribT') displayed a fairly linear behaviour until failure. Specimen 'AF-ribT-1' as the only exception exhibited two distinct drops of the applied force and a decrease of the flexural stiffness before reaching the ultimate load. The concrete beams with the flat reinforcement (without any bond enhancing features) collapsed at a considerably lower peak load, despite having the highest reinforcement ratio. The flexural stiffness of these two corresponding twins displayed a relatively large difference compared to the lower scatter in the other configurations. Specimen 'AF-flat-2' exhibited a steep drop of load and a subsequent load increase to approximately the same peak load at failure.

The crack patterns shortly before failure, as illustrated in Fig. 14, revealed that only four cracks had formed within the constant moment zone of Specimen 'AF-flat-1', whereby most of the deformations concentrated in two cracks. These substantial crack openings presumably caused a premature debonding of the reinforcement, leading to the lower stiffness of the reinforcement and causing the eventual collapse due to the complete delamination of the textile up to the end anchorage outside the supports. On the other hand, its twin 'AF-flat-2' exhibited a more uniform behaviour with multiple cracks forming within the constant moment zone. However, the failure also occurred due to the delamination of the reinforcement in a combined bending-shear crack just outside the constant moment zone, as shown in Fig. 14. The ultimate loads of these two specimens (M_u = {0.78; 0.70} kNm) were below that of the reference specimen with the standard rib layout (M_u = 0.85 kNm, see Fig. 7).

Most specimens with bond ribs failed in shear without prior announcement of the collapse. The higher number of ribs ('rib+') led to a considerable increase of the ultimate load compared to the flat reinforcement (in average + 39%), and to a lesser degree when compared to the standard rib layout reported in [20] (+21%). The specimens still failed due to the formation of a delamination crack along the reinforcement in the shear span since the connection of the ribs to the base textile remained a weak spot, similarly as shown in Fig. 9c. The introduction of transverse inlays ('ribX') prevented the textile rupture at the rib connection. However, the failure of the rib connections still happened between two transverse inlays, which had an average spacing of 30 mm. Since the textile reinforcement itself exhibits nearly no flexural stiffness, there was hardly any contribution to the shear resistance from dowel action and the textile delaminated over a short length, as illustrated in Fig. 15a. Therefore, the increase of ultimate load compared to the flat reinforcement was in a similar range as in Specimens 'AF-rib+' (+15%). The taller rib height ('ribT') significantly increased the failure load of the specimens. Specimen 'AF-ribT-2' still failed in shear, but with an increase of the ultimate load of 84% when compared to the

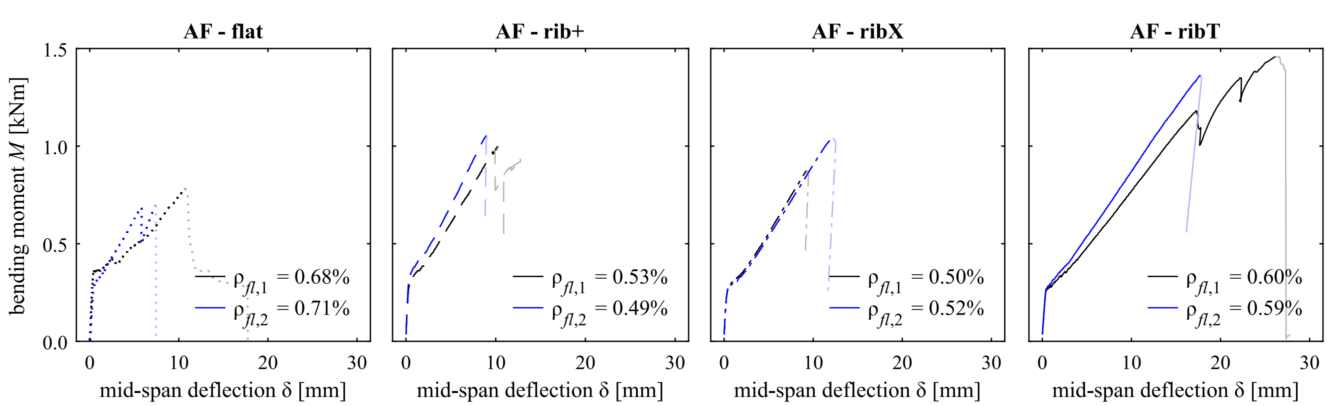

Fig. 13. Bending moment vs mid-span deflection of weft-knitted textile reinforced concrete beams with various rib geometries.

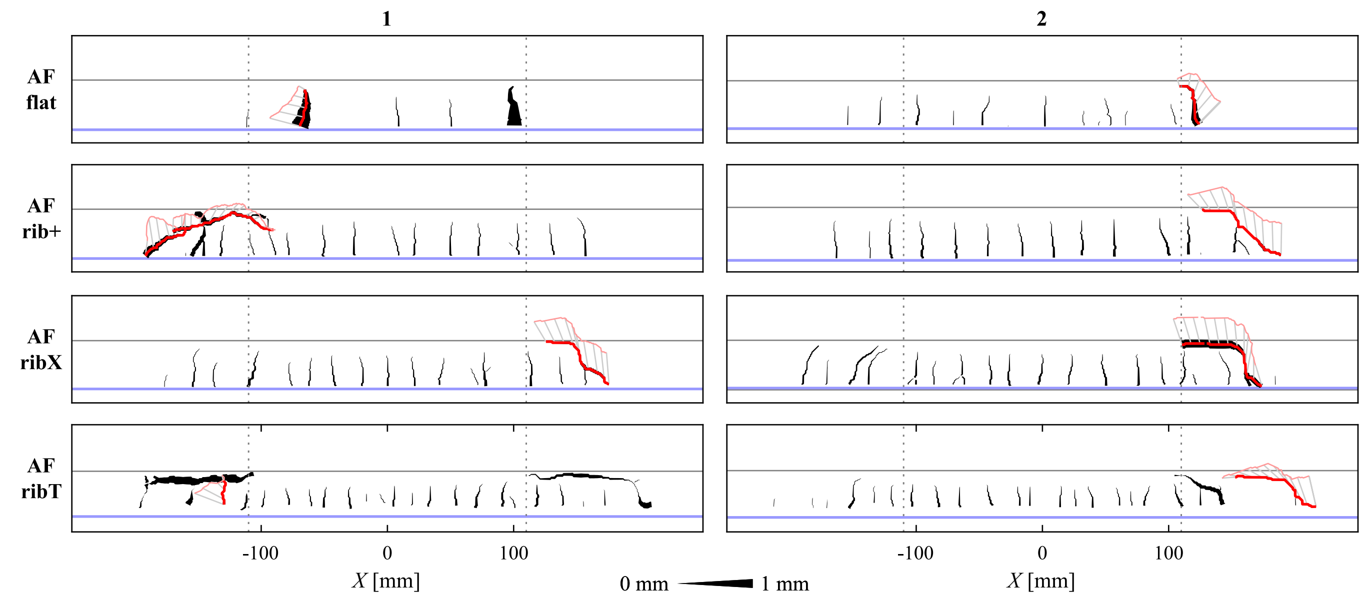

Fig. 14. Crack patterns shortly before failure for all weft-knitted textile reinforced concrete beams with various rib geometries (thickness of contours corresponding to crack width; governing crack marked in red with normalised displacement vector in grey and rose lines). (For interpretation of the references to colour in this figure legend, the reader is referred to the web version of this article.)

flat reinforcement. The reinforcement did not delaminate thanks to the deep anchorage of the ribs within the concrete element, but the inlays had ruptured due to the vertical opening of the shear crack, as shown in Fig. 15b. The textile reinforcement of 'AF-ribT-1' reached the full tensile resistance with the inlays rupturing in the governing bending crack, as illustrated in Fig. 15c. Compared to the flat textiles, this specimen presented an increase of the ultimate load of 97%. The drops in the applied load prior to failure originated from the formation of two major cracks in both shear spans (see Fig. 14; note that there are no DIC measurements in the lower part of the beams with tall ribs due to the rough surface, as described in Section 3.1). The progression of the shear crack in the left shear span into the compression zone locally reduced the height of the beam (Fig. 15c). Another shear crack formed in the opposite span soon after. Despite the substantial opening of this crack, the reinforcement did not delaminate, and the load increased again until eventually reaching the bending capacity. The governing bending crack did not lie in the constant moment zone but just outside the left shear span, where the compression zone was damaged.

4.3.2. *Response in the tension chord, crack behaviour and predictions from the tension chord Model*

All specimens with ribs exhibited a similar response in the tension chord regarding the stress–strain relationship (see Fig. 16a), with low scatter in the measurements of the Young's moduli (determined as described in Section 4.2.1 and summarised in Table 4). The observed tension stiffening effect in the experiments was in the upper range of the predictions using the Tension Chord Model (denoted as grey areas in Fig. 16a) and even slightly higher in some specimens. While Specimen 'AF-flat-1' displayed a similar stiffness as the textiles with bond ribs, Specimen 'AF-flat-2' exhibited significantly larger strains at the same stress level, reflecting the lower flexural stiffness observed in the moment-deflection curve.

The average crack widths (Fig. 16b) and the crack spacing (Fig. 16c) were in a close range for most specimens. The predictions from the Tension Chord Model slightly overestimated the crack spacings and consequently the crack widths. Specimen 'AF-flat-1' exhibited a considerably larger average crack width already at low load levels due to the early delamination of the textile.

5. Conclusions

This study investigated the influence of short integral glass fibres and spatial features to improve the structural performance of concrete beams with weft-knitted textile reinforcement attached to the bottom edge of the specimens, especially regarding their shear strength and their resistance against delamination of the reinforcement. To this end, an

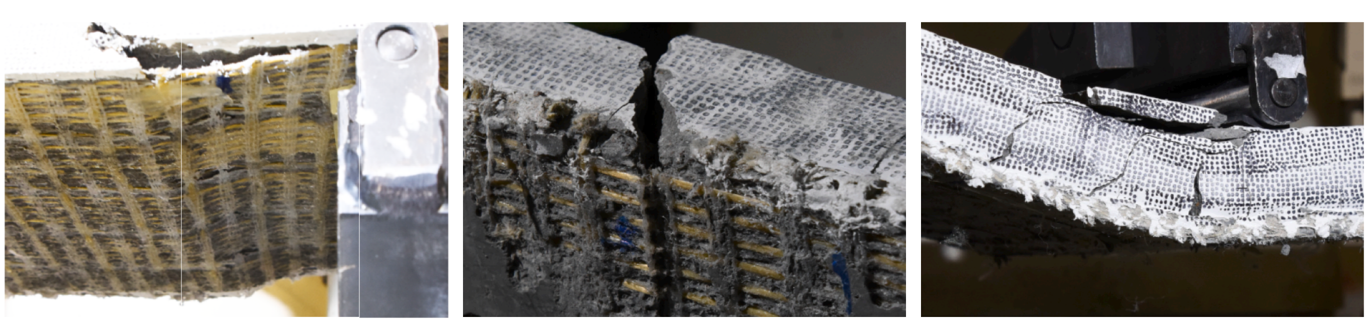

(a) (b) (c)

Fig. 15. Failure modes of weft-knitted textile reinforced concrete specimens with various rib geometries: (a) rupture of rib connection between transverse inlays ('AF-ribX-1'); (b) rupture of aramid inlays due to shear crack ('AF-ribT-2'); (c) bending failure due to concrete crushing and rupture of textile reinforcement ('AF-ribT-1').

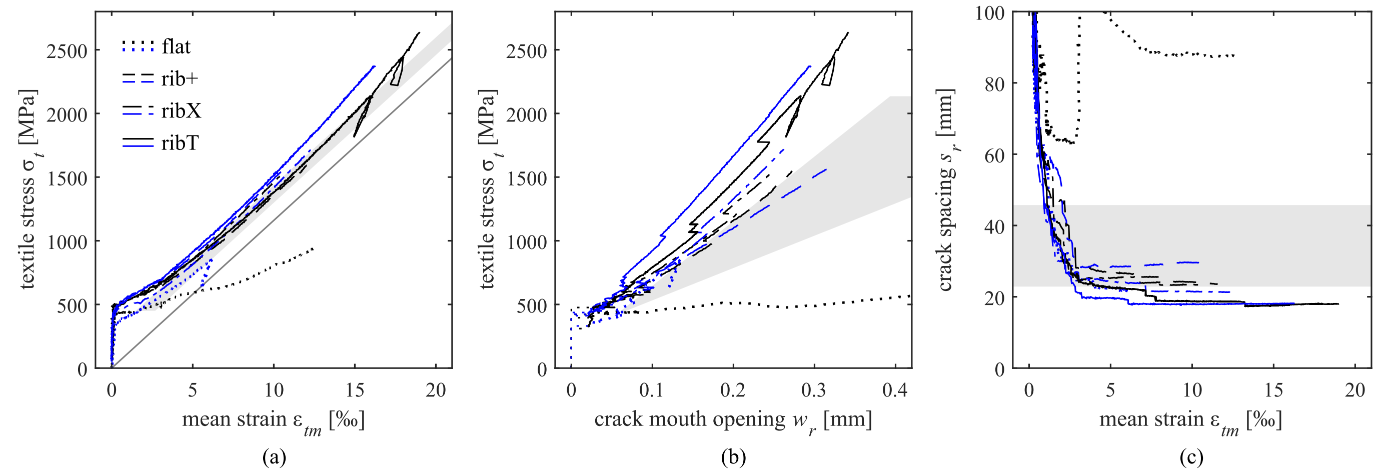

Fig. 16. Response in the tension chord within the constant moment zone of weft-knitted textile reinforced concrete beams with various rib geometries – experimental results and predictions using the Tension Chord Model (denoted as grey areas): (a) textile stress vs mean strains; (b) textile stress vs average crack mouth opening; (c) crack spacing vs mean strains.

experimental campaign consisting of 14 four-point-bending tests was carried out. The mechanical behaviour was examined regarding the load–deflection curves, the stress–strain relationship of the textile reinforcement and the crack kinematics based on the digital image correlation measurements, following the methodology presented in [20] to assess the response of the tension chord for concrete members subjected to bending.

The introduction of bond ribs in the textile was seen to be essential to provide a mechanical interlock that prevents or delays the delamination of the bottom reinforcement. The ribs with a height of 30 mm (i.e. ca. 75% of the height of the beams) prevented the delamination of the reinforcement. These tall ribs effectively bridged the shear crack, acting as integrated stirrups. This allowed the load-bearing capacity to be increased by 97% with respect to the beams without bond ribs. Other rib layouts had a significantly lesser impact in increasing the shear resistance due to the low height of the ribs, which either failed at the connection between the rib and the base textile, or broke out of the concrete. The strengthening of the rib connections using transverse inlays had only little effect since the low flexural stiffness of the longitudinal reinforcement itself allowed the delamination of the textile over a short length between two transverse rovings. Despite not being able to avoid the delamination of the reinforcement, these bond rib configurations were still able to delay the delamination and considerably increase the load reached by the beams with flat reinforcement without spatial features, which failed prematurely with very low utilisation of the inlays.

The addition of short integral glass fibres to specimens with bond ribs of 5 mm in height (ca. 12% of the depth of the beams) did not prevent the delamination failure and only slightly increased the load-bearing capacity. However, the serviceability behaviour was significantly improved, with a reduction of ca. 29% in deflections and 35% in crack widths at 60% of the ultimate load of the reference specimen without short fibres. The contribution of the short glass fibres to the load-deformation and crack behaviour of the weft-knitted textile reinforced concrete beams were estimated using Pfyl's fibre engagement model [31]. The fibre effectiveness and the pull-out length were determined from experiments on fibre reinforced concrete beams without textile reinforcement. The resulting effective fibre stress-crack opening relationship was in a reasonable range compared to similar fibre reinforced concrete mixes with short integral glass fibres found in the literature. However, the pull-out resistance was considerably lower when compared to steel fibre reinforced concrete with a similar fibre volumetric content since short integral glass fibres may break prematurely due to sharp curvatures at the crack edges or partial pull-out of the fibre core from the sleeve. The contribution of the fibres to the bending moment of the weft-knitted textile reinforced concrete beams were the highest just after cracking (roughly 70% contribution) and naturally decreased with increasing load due to the widening of the bending cracks (only around 8% contribution at ultimate load). These results indicate that the influence of the short fibres may vanish for load levels where the textile reinforcement would reach its tensile strength. However, all beams failed prematurely due to the delamination of the reinforcement with only a slight increase of the shear resistance when compared to the reference specimen without short fibres. Although the fibres may contribute to the stress transfer over diagonal shear cracks, most of the governing cracks exhibited a steep inclination, resulting in a predominantly sliding motion, limiting the effect of the fibres. The use of short dispersed fibres instead of integral ones may influence the cracking behaviour as reported in the literature, especially regarding the shear transfer across the governing crack, which needs to be investigated in further research.

The type of material for the textile reinforcement (AF, CF or GF) did not have a significant influence on the general mechanical response – except the flexural stiffness due to the different Young's moduli – as all specimens exhibited a similar load-deformation behaviour and failed prematurely in shear, whereby the specimens with aramid inlays exhibited the highest utilisation of the textile strength at the ultimate load.

Predicting the stress–strain relationship of the tension chord and the average crack widths using the Tension Chord Model yielded a good correlation between model and experiments for all tested beams (with and without short fibres), with all material parameters being determined a priori in separate tests, which proved the applicability of this approach to various textile materials and rib types.

A key finding of this study is that the introduction of continuous spatial features connected to the weft-knitted textile reinforcement was the most effective for preventing the premature collapse mechanism. Future studies may investigate the variation of the rib height and spacing to optimise materials use. As the manufacturing procedure using a CNC knitting machine opens innumerable possibilities for bespoke geometries, more complex structures (e.g. curved or folded) and loading conditions (such as two-way bending, membrane forces or in-plane shear) should be the subject of further research to fully exploit the potential of weft-knitted textile reinforcement. Furthermore, future steps in the development of the presented novel type of stay-in-place formwork with integrated textile reinforcement will need to address the robustness and durability against potentially damaging conditions due to the absence of the concrete cover.

CRediT authorship contribution statement

Minu Lee: Conceptualization, Methodology, Investigation, Visualization, Writing – original draft. **Jaime Mata-Falcón:** Conceptualization, Methodology, Writing – review & editing, Supervision. **Walter Kaufmann:** Conceptualization, Writing – review & editing, Funding acquisition.

Declaration of Competing Interest

The authors declare that they have no known competing financial interests or personal relationships that could have appeared to influence the work reported in this paper.

Data availability

The experimental data presented in this article was submitted to a public data repository and is published under the following DOI: 10.3929/ethz-b-000535030

Acknowledgements

The authors gratefully acknowledge Dr Mariana Popescu from Block Research Group (ETHZ) and Dr Lex Reiter from the Chair of Physical Chemistry of Building Materials (ETHZ) for contributing their technical and practical expertise as well as the students Nathalie Chiaverio and Caterina Rovati for their valuable support during preparation and testing of the specimens shown in this paper. This research is supported by the National Centre for Competence in Research in Digital Fabrication, funded by the Swiss National Science Foundation (project number 51NF40-141853).

Open access data

The experimental data presented in this article was submitted to a public data repository and is published under the following https://doi.org/10.3929/ethz-b-000535030.

Appendix. Derivation of bending resistance of weft-knitted textile reinforced concrete with short fibres

Crack opening u at height z of the cross-section for linearly opening bending crack for given crack mouth opening w_r:

$$u(z) = \frac{w_r}{h - x_c} \cdot z$$

Concrete tensile stresses for a linearly opening bending crack:

$$\sigma_{cf}(z) = \sigma_{cf0} \cdot \left(1 - \frac{2 \cdot u(z)}{l_f}\right)^2 = \sigma_{cf0} \cdot \left(1 - \frac{2 \cdot w_r}{l_f \cdot (h - x_c)} \cdot z\right)^2 = \sigma_{cf0} \cdot \left(1 - \frac{\xi}{h - x_c} \cdot z\right)^2$$

with.

$$\xi = \frac{2 \cdot w_r}{l_f}$$

Mean concrete tensile stresses due to fibres for given crack mouth opening w_r:

$$\sigma_{cfm} = \frac{1}{h - x_c} \cdot \int_0^{h - x_c} \sigma_{cf}(u) \cdot dz = \frac{1}{h - x_c} \cdot \int_0^{h - x_c} \sigma_{cf0} \cdot \left(1 - \frac{\xi}{h - x_c} \cdot z\right)^2 \cdot dz = \sigma_{cf0} \cdot \frac{\xi^2 - 3 \cdot \xi + 3}{3}$$

Position of resultant of effective fibre stresses measured from center of compression force ($x/3$):

$$\begin{aligned} \varsigma_{cf} &= \frac{1}{\sigma_{cfm} \cdot (h - x_c)} \cdot \int_0^{h - x_c} \sigma_{cf}(z) \cdot z \cdot dz + \frac{2 \cdot x_c}{3} = \frac{1}{\sigma_{cfm} \cdot (h - x_c)} \cdot \int_0^{h - x_c} \sigma_{cf0} \cdot \left(1 - \frac{\xi}{h - x_c} \cdot z\right) \cdot z \cdot dz + \frac{2 \cdot x_c}{3} \\ &= (h - x_c) \cdot \frac{3 \cdot \xi^2 - 8 \cdot \xi + 6}{4 \cdot \xi^2 - 3 \cdot \xi + 3} + \frac{2 \cdot x_c}{3} \end{aligned}$$

Contribution of fibres to bending resistance for given crack mouth opening w_r:

$$M = b \cdot (h - x_c) \cdot \sigma_{cfm} \cdot \varsigma_{cf} = b \cdot (h - x_c) \cdot \sigma_{cf0} \cdot \frac{\xi^2 - 3 \cdot \xi + 3}{3} \cdot \left(\frac{3 \cdot \xi^2 - 8 \cdot \xi + 6}{12 \cdot \xi^2 - 3 \cdot \xi + 3} \cdot (h - x_c) + \frac{2 \cdot x_c}{3}\right)$$

References

[1] V. Mechtcherine, Towards a durability framework for structural elements and structures made of or strengthened with high-performance fibre-reinforced composites, Constr. Build. Mater. 31 (2012) 94–104, https://doi.org/10.1016/j.conbuildmat.2011.12.072.

[2] International Union of Laboratories and Experts in Construction Materials, Systems and Structures, Brameshuber W, editors. State-of-the-Art report of RILEM Technical Committee TC 201-TRC “Textile Reinforced Concrete.” Bagneux: RILEM Publ; 2006.

[3] M. Curbach (Ed.), Sachstandbericht zum Einsatz von Textilien im Massivbau, Beuth, Berlin, 1998.

[4] M. Curbach, F. Jesse, Eigenschaften und Anwendung von Textilbeton, Eigenschaften und Anwendung von Textilbeton. BUST 104 (1) (2009) 9–16.

[5] J. Hegger, N. Will, O. Bruckermann, S. Voss, Load–bearing behaviour and simulation of textile reinforced concrete, Mater Struct 39 (2006) 765–776, https://doi.org/10.1617/s11527-005-9039-y.

[6] J. Hegger, M. Horstmann, S. Voss, N. Will, Textilbewehrter Beton: Tragverhalten, Bemessung und Anwendung, Beton- Stahlbetonbau 102 (2007) 362–370, https://doi.org/10.1002/best.200700552.

[7] P. Valeri, M. Fernàndez Ruiz, A. Muttoni, Tensile response of textile reinforced concrete, Constr. Build. Mater. 258 (2020), 119517, https://doi.org/10.1016/j.conbuildmat.2020.119517.

[8] M. Alvarez, Einfluss des Verbundverhaltens auf das Verformungsvermögen von Stahlbeton, vol. 236, Birkhäuser, Basel, Switzerland, 1998.

[9] J. Hegger, O. Bruckermann, R. Chudoba, A smeared bond-slip relation for multi-filament yarns embedded in fine concrete, RILEM Publications SARL, Varenna, 2004, pp. 1453–1462.

[10] B. Banholzer, T. Brockmann, W. Brameshuber, Material and bonding characteristics for dimensioning and modelling of textile reinforced concrete (TRC)

elements, Mater Struct 39 (2006) 749–763, https://doi.org/10.1617/s11527-006-9140-x.
[11] U. Häußler-Combe, J. Hartig, Bond and failure mechanisms of textile reinforced concrete (TRC) under uniaxial tensile loading, Cem. Concr. Compos. 29 (2007) 279–289, https://doi.org/10.1016/j.cemconcomp.2006.12.012.
[12] E. Mader, R. Plonka, M. Schiekel, R. Hempel, Coatings on Alkali-Resistant Glass Fibres for the Improvement of Concrete, J. Ind. Text. 33 (2004) 191–207, https://doi.org/10.1177/1528083704039833.
[13] M. Glowania, T. Gries, J. Schoene, M. Schleser, U. Reisgen, Innovative Coating Technology for Textile Reinforcements of Concrete Applications, KEM 466 (2011) 167–173, https://doi.org/10.4028/www.scientific.net/kem.466.167.
[14] T. Quadflieg, S. Leimbrink, T. Gries, O. Stolyarov, Effect of coating type on the mechanical performance of warp-knitted fabrics and cement-based composites, J. Compos. Mater. 52 (2018) 2563–2576, https://doi.org/10.1177/0021998317750003.
[15] M. Popescu, M. Rippmann, T. Van Mele, P. Block, Automated Generation of Knit Patterns for Non-developable Surfaces, in: K. De Rycke, C. Gengnagel, O. Baverel, J. Burry, C. Mueller, M.M. Nguyen, P. Rahm, M.R. Thomsen (Eds.), Humanizing Digital Reality, Springer Singapore, Singapore, 2018, pp. 271–284.
[16] M. Popescu, L. Reiter, A. Liew, T. Van Mele, R.J. Flatt, P. Block, Building in Concrete with an Ultra-lightweight Knitted Stay-in-place Formwork: Prototype of a Concrete Shell Bridge, Structures 14 (2018) 322–332, https://doi.org/10.1016/j.istruc.2018.03.001.
[17] M. Popescu, M. Rippmann, A. Liew, L. Reiter, R.J. Flatt, T. Van Mele, P. Block, Structural design, digital fabrication and construction of the cable-net and knitted formwork of the KnitCandela concrete shell, Structures 31 (2021) 1287–1299, https://doi.org/10.1016/j.istruc.2020.02.013.
[18] Potential Approaches for Reinforcing Complex Concrete Structures with Integrated Flexible Formwork vol. 28 (2020) 669–679, https://doi.org/10.1007/978-3-030-49916-7_67.
[19] M. Lee, J. Mata-Falcón, W. Kaufmann, Load-deformation behaviour of weft-knitted textile reinforced concrete in uniaxial tension, Mater Struct 54 (2021) 210, https://doi.org/10.1617/s11527-021-01797-5.
[20] M. Lee, J. Mata-Falcón, W. Kaufmann, Analysis of the tension chord in the flexural response of concrete elements: Methodology and application to weft-knitted textile reinforcement, Eng. Struct. 261 (2022) 114270, https://doi.org/10.1016/j.engstruct.2022.114270.
[21] R. Barhum, V. Mechtcherine, Effect of short, dispersed glass and carbon fibres on the behaviour of textile-reinforced concrete under tensile loading, Eng. Fract. Mech. 92 (2012) 56–71, https://doi.org/10.1016/j.engfracmech.2012.06.001.
[22] R. Barhum, V. Mechtcherine, Influence of short dispersed and short integral glass fibres on the mechanical behaviour of textile-reinforced concrete, Mater Struct 46 (2013) 557–572, https://doi.org/10.1617/s11527-012-9913-3.
[23] Y. Du, X. Zhang, L. Liu, F. Zhou, D. Zhu, W. Pan, Flexural Behaviour of Carbon Textile-Reinforced Concrete with Prestress and Steel Fibres, Polymers 10 (2018) 98, https://doi.org/10.3390/polym10010098.
[24] D. Zhu, S. Liu, Y. Yao, G. Li, Y. Du, C. Shi, Effects of short fiber and pre-tension on the tensile behavior of basalt textile reinforced concrete, Cem. Concr. Compos. 96 (2019) 33–45, https://doi.org/10.1016/j.cemconcomp.2018.11.015.
[25] H. Li, S. Liu, G. Li, Y. Yao, C. Shi, Y. Ou, et al., Flexural Performance of Basalt Textile-Reinforced Concrete with Pretension and Short Fibers, J. Mater. Civ. Eng. 32 (2020) 04020004, https://doi.org/10.1061/(ASCE)MT.1943-5533.0003077.
[26] A. Amin, S.J. Foster, A. Muttoni, Derivation of the σ- w relationship for SFRC from prism bending tests, Structural Concrete 16 (2015) 93–105, https://doi.org/10.1002/suco.201400018.
[27] A. Roye, T. Gries, 3-D Textiles for Advanced Cement Based Matrix Reinforcement, J. Ind. Text. 37 (2007) 163–173, https://doi.org/10.1177/1528083707078136.
[28] R. Haik, E. Adiel Sasi, A. Peled, Influence of three-dimensional (3D) fabric orientation on flexural properties of cement-based composites, Cem. Concr. Compos. 80 (2017) 1–9, https://doi.org/10.1016/j.cemconcomp.2017.02.007.
[29] El Kadi M, Tysmans T, Verbruggen S, Vervloet J, De Munck M, Wastiels J, et al. Experimental study and benchmarking of 3D textile reinforced cement composites. Cement and Concrete Composites 2019;104:103352. https://doi.org/10.1016/j.cemconcomp.2019.103352.
[30] T. Markić, A. Amin, W. Kaufmann, T. Pfyl, Strength and Deformation Capacity of Tension and Flexural RC Members Containing Steel Fibers, J. Struct. Eng. 146 (2020) 04020069, https://doi.org/10.1061/(ASCE)ST.1943-541X.0002614.
[31] Pfyl T. Tragverhalten von Stahlfaserbeton. Doctoral Thesis. ETH Zurich, 2003. https://doi.org/10.3929/ethz-a-004502831.
[32] P. Marti, M. Alvarez, W. Kaufmann, V. Sigrist, Tension chord model for structural concrete, Structural Engineering International 8 (1998) 287–298, https://doi.org/10.2749/101686698780488875.
[33] A. Amin, R.I. Gilbert, Steel Fiber-Reinforced Concrete Beams—Part I: Material Characterization and In-Service Behavior, SJ 116 (2019) 101–111, https://doi.org/10.14359/51713288.
[34] Barros JAO, Figueiras JA, Veen CDV. Tensile behaviour of glass fibre reinforced concrete. In: Silva Gomes JF, editor. Recent Advances in Experimental Mechanics, Lisbon, Portugal: 1994, p. 1073–80.
[35] T.S. Ng, T. Htut, S. Foster, Fracture of Steel Fibre Reinforced Concrete –. The Unified Variable Engagement Model, School of Civil and Environmental Engineering, The University of New South Wales, Sydney, Australia, 2012.
[36] S.-C. Lee, J.-Y. Cho, F.J. Vecchio, Diverse Embedment Model for Steel Fiber-Reinforced Concrete in Tension: Model Development, MJ 108 (2011) 516–525. https://doi.org/10.14359/51683261.
[37] J.G.M. van Mier, M.R.A. van Vliet, Uniaxial tension test for the determination of fracture parameters of concrete: state of the art, Eng. Fract. Mech. 69 (2002) 235–247, https://doi.org/10.1016/S0013-7944(01)00087-X.
[38] P. Pujadas, A. Blanco, S.H.P. Cavalaro, A. de la Fuente, A. Aguado, Multidirectional double punch test to assess the post-cracking behaviour and fibre orientation of FRC, Constr. Build. Mater. 58 (2014) 214–224, https://doi.org/10.1016/j.conbuildmat.2014.02.023.
[39] International Federation for Structural Concrete, fib model code for concrete structures 2010, Ernst & Sohn, Berlin, 2013.
[40] Kuuskoski V. Über die Haftung zwischen Beton und Stahl. Doctoral Thesis. The State Institute for Technical Research, 1950.
[41] G. Rehm, Über die Grundlagen des Verbundes zwischen Stahl und Beton vol. Heft 138 (1961) p. 59 pp..
[42] Galkovski T, Mata-Falcón J, Kaufmann W. Effective reinforcement ratio of RC beams: Validation of modelling assumptions with high-resolution strain data. Structural Concrete 2022:suco.202100739. https://doi.org/10.1002/suco.202100739.
[43] P. Marti, Reinforced Concrete I Lecture Notes, Department of Civil, Environmental and Geomatic Engineering, ETH Zurich, 2004.
[44] C. Burns, Serviceability analysis of reinforced concrete based on the tension chord model, ETH Zürich (2012), https://doi.org/10.3929/ethz-a-009753066.
[45] R&G Faserverbundwerkstoffe GmbH, Technische Daten -, Epoxydharz L (2020).
[46] Owens Corning, CEM-FIL(R) 62: AR-Schnittglasfasern für Trockenmörtel und GRC-Premix - Produktdatenblatt, Owens Corning Composite Materials, LLC. (2016).
[47] DIN, DIN EN 196–1:2016–11, Prüfverfahren für Zement_- Teil_1: Bestimmung der Festigkeit; Deutsche Fassung EN_196-1:2016, Beuth Verlag GmbH (2016), https://doi.org/10.31030/2482416.
[48] Correlated Solutions. Vic-3D Software Manual. Correlated Solutions Inc.; 2019.
[49] Fachbereich Prozessmesstechnik und Strukturanalyse. VDI/VDE 2626 Blatt 1 - Optische Messverfahren - Bildkorrelationsverfahren - Grundlagen und Begriffe. VDI/VDE-Gesellschaft Mess- und Automatisierungstechnik; 2018.
[50] J. Mata-Falcón, S. Haefliger, M. Lee, T. Galkovski, N. Gehri, Combined application of distributed fibre optical and digital image correlation measurements to structural concrete experiments, Eng. Struct. 225 (2020), 111309, https://doi.org/10.1016/j.engstruct.2020.111309.
[51] N. Gehri, J. Mata-Falcón, W. Kaufmann, Automated crack detection and measurement based on digital image correlation, Constr. Build. Mater. 256 (2020), 119383, https://doi.org/10.1016/j.conbuildmat.2020.119383.
[52] N. Gehri, J. Mata-Falcón, W. Kaufmann, Refined extraction of crack characteristics in Large-scale concrete experiments based on digital image correlation, Eng. Struct. 251 (2022), 113486, https://doi.org/10.1016/j.engstruct.2021.113486.
[53] W. Kaufmann, A. Amin, A. Beck, M. Lee, Shear transfer across cracks in steel fibre reinforced concrete, Eng. Struct. 186 (2019) 508–524, https://doi.org/10.1016/j.engstruct.2019.02.027.
[54] P. Stähli, R. Custer, J.G.M. van Mier, On flow properties, fibre distribution, fibre orientation and flexural behaviour of FRC, Mater. Struct. 41 (2008) 189–196, https://doi.org/10.1617/s11527-007-9229-x.
[55] Q. Zhang, S. Li, S. Gong, G. Zhang, G. Xi, Y. Wu, Study on Flexural Properties of Basalt Fiber Textile Reinforced Concrete (BTRC) Sheets Including Short AR-Glass Fibers, Front. Mater. 7 (2020) 277, https://doi.org/10.3389/fmats.2020.00277.